

**RL-TR-96-109**  
**Final Technical Report**  
**June 1996**



# **FINITE ELEMENT MODELING AND ANALYSIS OF MCM HIGH DENSITY INTERCONNECT VIAS**

**University of Massachusetts**

**I. Grosse and J. DiTomaso**

*APPROVED FOR PUBLIC RELEASE; DISTRIBUTION UNLIMITED.*

**19960805 043**

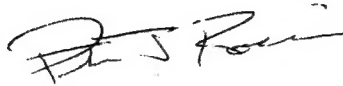
**Rome Laboratory  
Air Force Materiel Command  
Rome, New York**

**DTIC QUALITY INSPECTED A**

This report has been reviewed by the Rome Laboratory Public Affairs Office (PA) and is releasable to the National Technical Information Service (NTIS). At NTIS, it will be releasable to the general public, including foreign nations.

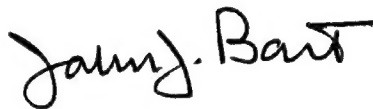
RL-TR- 96-109 has been reviewed and is approved for publication.

APPROVED:



PETER J. ROCCI  
Project Engineer

FOR THE COMMANDER:



JOHN J. BART  
Chief Scientist, Reliability Sciences  
Electromagnetics & Reliability Directorate

If your address has changed or if you wish to be removed from the Rome Laboratory mailing list, or if the addressee is no longer employed by your organization, please notify Rome Laboratory/ ( ERDS ), Rome NY 13441. This will assist us in maintaining a current mailing list.

Do not return copies of this report unless contractual obligations or notices on a specific document require that it be returned.

# REPORT DOCUMENTATION PAGE

Form Approved  
OMB No. 0704-0188

Public reporting burden for this collection of information is estimated to average 1 hour per response, including the time for reviewing instructions, searching existing data sources, gathering and maintaining the data needed, and completing and reviewing the collection of information. Send comments regarding this burden estimate or any other aspect of this collection of information, including suggestions for reducing this burden, to Washington Headquarters Services, Directorate for Information Operations and Reports, 1215 Jefferson Davis Highway, Suite 1204, Arlington, VA 22202-4302, and to the Office of Management and Budget, Paperwork Reduction Project (0704-0188), Washington, DC 20503.

1. AGENCY USE ONLY (Leave Blank)		2. REPORT DATE June 1996		3. REPORT TYPE AND DATES COVERED Final Apr 94 - Apr 95	
4. TITLE AND SUBTITLE Finite Element Modeling and Analysis of MCM High Density Interconnect Vias				5. FUNDING NUMBERS C - F30602-94-C-0067 PE - 62702F PR - 2338 TA - 02 WU - PM	
6. AUTHOR(S) I. Grosse and J. DiTomasso					
7. PERFORMING ORGANIZATION NAME(S) AND ADDRESS(ES) University of Massachusetts Department of Mechanical & Industrial Engineering Amherst MA 01003				8. PERFORMING ORGANIZATION REPORT NUMBER  N/A	
9. SPONSORING/MONITORING AGENCY NAME(S) AND ADDRESS(ES)  Rome Laboratory/ERDS 525 Brooks Rd Rome NY 13441-4505				10. SPONSORING/MONITORING AGENCY REPORT NUMBER  RL-TR-96-109	
11. SUPPLEMENTARY NOTES  Rome Laboratory Project Engineer: Peter R. Rocci/ERDS/(315) 330-4891					
12a. DISTRIBUTION/AVAILABILITY STATEMENT  Approved for public release; distribution unlimited.				12b. DISTRIBUTION CODE	
13. ABSTRACT (Maximum 200 words)  Failure modes of vias within a chip's first multi-chip module are studied using several two and three-dimensional families of finite element models. The models study both the global strains of the entire module and local strains of a single via under uniform temperature loading between -65°C and 120°C. The accuracy of the models was verified by comparing different families of models with each other, with analytical beam theory, and with empirical data generated by electron beam moire strain data taken by NIST on a test specimen. Global finite element analysis results revealed that the strains within the high density interconnect layer have only a 10% effect upon the local via strains. A simple analytical method was developed to obtain displacement boundary conditions to be applied to local via finite element models, thereby precluding the need for global finite element analysis of the entire module. For a local via analysis, the axisymmetric and three-dimensional finite element models were found to predict the location of via failures, which agrees with failure locations observed under accelerated test conditions. A number of via design factors were identified that affect the strain concentration in the via wall. However, the dielectric/epoxy intermaterial boundary was not found to be the cause of the strain concentration in the via wall.					
14. SUBJECT TERMS Finite element analysis, Multichip modules, High density interconnect vias				15. NUMBER OF PAGES 102	
				16. PRICE CODE	
17. SECURITY CLASSIFICATION OF REPORT UNCLASSIFIED	18. SECURITY CLASSIFICATION OF THIS PAGE UNCLASSIFIED	19. SECURITY CLASSIFICATION OF ABSTRACT UNCLASSIFIED	20. LIMITATION OF ABSTRACT  UL		

## EXECUTIVE SUMMARY

The failure modes of vias within a chips first multi-chip module are studied using several two and three-dimensional families of finite element models. The models study both the global strains of the entire module and local strains of a single via under uniform temperature loading between -65 °C and 120 °C. The accuracy of the models are verified by comparing different families of models with each other, analytical beam theory and empirical data generated by electron beam moiré.

The strains within the high density interconnect layer that contain the vias are dominated by the stiff alumina substrate and the silicon chips. The total global strain in the interconnect layer can be bounded by zero and the thermal expansion of the substrate. However these bounding strains have only a 10% effect upon the via strain. Hence it is not necessary to construct a global model for the purpose of applying boundary conditions to local via models.

Axisymmetry is found to be the best two-dimensional assumption for a local via model. The axisymmetric analysis predicts the location of via failure, and its results agree with the three-dimensional model results within 10%. Two-dimensional plane stress or plane strain models under predict the elastic strain by as much as 40%. This difference is caused by the bending loads created by the top landing pad and the coefficient of thermal

expansion mismatch between the dielectric, epoxy, and copper. A plane stress/strain model models the via wall as a sheet which is very compliant in bending. The actual via geometry and the axisymmetric model is much stiffer in bending. Thus, it generates larger strains in bending.

The models predict that the via should fail in the lower part of the inside via wall in the corner, which agrees with failures observed under accelerated test conditions (no failures have been observed under normal operating conditions). The models also predict that the entire via wall yields at -65 °C and 120 °C.

Factors (other than the fundamental driving mechanism of CTE mismatch between the polymers and copper material) identified as increasing in the strain in the via wall are 1) increasing the stiffness of the material below the via, 2) increasing the steepness of the via wall, 3) decreasing the thickness of the via wall, and 4) increasing the thickness of the top pad. However, the dielectric/epoxy intermaterial boundary outside the via wall *was not found* to be a cause of the high strain concentration in the via barrel as originally suspected.

## TABLE OF CONTENTS

	<u>Page</u>
EXECUTIVE SUMMARY .....	i
LIST OF TABLES .....	v
LIST OF FIGURES .....	vi
 Chapter	
1. INTRODUCTION .....	1
1.1 What is a MCM? .....	1
1.2 Via Reliability .....	2
1.3 The Analysis .....	3
1.4 Objectives .....	4
2. RELATED WORK .....	6
2.1 Via Hole Failure Study, by A. Isobe <i>et al</i> .....	6
2.2 A Thermo-Mechanical Fatigue Analysis of HDI Vias, by Prabhu <i>et al</i> ..	7
2.3 Chapter Summary .....	11
3. GLOBAL ANALYSIS .....	13
3.1 Two-Dimensional Finite Element Model .....	14
3.2 Two-Dimensional Analytical Model .....	20
3.3 Limitations of a Two-Dimensional Approach .....	24
3.4 Shell Model Finite Element Analysis .....	24
3.5 Application to a Three-Dimensional Analysis .....	27
3.6 Chapter Summary .....	28
4. LOCAL VIA MODELS .....	38
4.1 Family of Axisymmetric Finite Element Models .....	38
4.2 Family of Three-Dimensional Finite Element Models .....	47
4.3 Chapter Summary .....	49
5. EMPIRICAL CALIBRATION .....	57
5.1 Empirical Technique .....	57

5.2	Data Reduction .....	59
5.3	Modeling Technique .....	60
5.4	Discussion .....	60
5.5	Chapter Summary .....	63
6.	MODELING GUIDELINES .....	70
6.1	Global Models .....	70
6.2	Isotropic vs. Orthotropic Material Properties .....	71
6.3	Plane Strain, Plane Stress or Axisymmetry .....	71
6.4	Linear vs. Non-Linear Analyses .....	72
6.5	Via Stress Variation with Location .....	72
6.6	Model Verification and Calibration .....	73
7.	CONCLUSIONS .....	74
APPENDICES		
A.	FINITE ELEMENT MODEL INFORMATION .....	77
B.	MATERIAL PROPERTIES .....	78
C.	DERIVATION OF THE ANALYTICAL MODEL .....	82
D.	DERIVATION OF VARIOUS FORMULA .....	86
BIBLIOGRAPHY .....		88

## LIST OF TABLES

Table	<u>Page</u>
1. Schematic showing a cutaway view of (a) a typical electronic package (b) a multi-chip module (MCM). .....	34
2. Components of the expansion coefficient derived from the two-dimensional analytical model. $\alpha_n$ is the component of expansion due to the neutral axis growth, $\alpha_b$ is the component of expansion due to bending and $\alpha_t$ is the total expansion. $\alpha_i$ is the CTE for layer	34
3. Parameter key for the two-dimensional family of via model	50
4. Stresses and Strains of two-dimensional family of via models at 120 °C. Results normalized to the maximum equivalent strain in the base model	54
5. Common model information for all the finite element models in this report	77
6. Unique model information for the finite element models in this report	77
7. Material property data used throughout this report	78



## LIST OF FIGURES

Figure	<u>Page</u>
1. Schematic showing a cutaway view of (a) a typical electronic package (b) a multi-chip module (MCM). ....	5
2. Schematic showing (a) the HDI layer within a MCM, and (b) a close up of the via structure within a MCM. ....	5
3. Schematic showing the via/landing pad peeling phenomenon reported by Isobe <i>et al</i> [3]. Note displacements are exaggerated. ....	12
4. Life vs. $\Delta T$ calculated with the Engelmaier model and a plane strain finite element analysis reported by Prabhu <i>et al</i> [4]. ....	12
5. Location of "slice" for the two-dimensional finite element model of the MCM. ....	30
6. Shell model schematic. ....	30
7. Model geometry for the two-dimensional finite element model. ....	31
8. Boundary conditions for the two-dimensional plane strain finite element model. ....	31
9. Element plot of the two-dimensional plane strain finite element model.	32
10. X Displacement vs. Z at 100 °C for the two-dimensional finite element MCM model. ....	32
11. X Strain vs. Z at 100 °C for the two-dimensional finite element MCM model. ....	33
12. X Strain vs. X. At the top and bottom of the HDI layers at 100 °C. ....	33
13. A cut away view of (a) a three-dimensional representation of the two-dimensional model, (b) a portion of an three-dimensional multi - chip module. ....	35
14. Geometry for the shell finite element model. ....	35

15. Shell model element plot with boundary conditions. ....	36
16. Z strain predicted from the two-dimensional model vs. the shell model. ....	36
17. Suggested boundary conditions for a three-dimensional local analysis. ....	37
18. Geometry of axisymmetric via model family. ....	51
19. Boundary conditions and element plot for the base axisymmetric via finite element model. ....	51
20. Effective structural strains in a via with the base geometry at 120 °C. ..	52
21. Plastic effective structural strains in a via with the base geometry at 120 °C. ....	52
22. Effective structural strain vs. Z location along the inside via wall. ....	53
23. Displacement plots of (a) level zero and (b) level one via. ....	53
24. Three-dimensional local via model element plot. ....	55
25. Elastic + Plastic von Mises strain in (a) the axisymmetric model, and (b) the three-dimensional model. ....	55
26. Plastic von Mises strain in (a) the axisymmetric model, and (b) the three-dimensional model. ....	56
27. The moiré fringe pattern at (a) 24 °C, and (b) 151 °C. ....	65
28. Normalized finite element z strains (i.e... total z expansion rate, $\alpha_{z\_tot}$ ) for a plane stress model with NIST geometry. ....	65
29. Data acquisition paths for emperical/analytical data comparisons. ....	66
30. EBM data vs. finite element analysis for path a/a' (Center of Via). ....	66
31. EBM data vs. finite element analysis for path c/c' (Near Via Inside Wall). ....	67
32. EBM data vs. finite element analysis for path h/h' (Outside of the Via). ....	67
33. EBM data vs. finite element analysis for path J (Through the Via Layer). ....	68
34. EBM data vs. finite element analysis for path P (Through the Epoxy Layer). ....	68

35. EBM data vs. finite element analysis for path U (Through the Top Kapton Layer). .....	69
36. True Stress vs. True Strain curves for Kapton. ....	79
37. True Stress vs. True Strain curves for Ultem. ....	79
38. True Stress vs. True Strain curves for SPI EPOXY. ....	80
39. True Stress vs. True Strain curves for SDAN. ....	80
40. True Stress vs. True Strain curves for SE45. ....	81
41. True Stress vs. True Strain curves for copper. ....	81
42. Schematic showing a portion of a generic layered solid in bending. ...	82

## **CHAPTER 1**

### **INTRODUCTION**

In order to understand the modes of failure of vias in Multi-Chip Modules (MCM) one must understand the function, the geometry, and the loads placed upon the via. However, before we can understand the local system, the via, we must understand the global system, the MCM.

#### **1.1 What is a MCM?**

MCMs are the next stage of evolution for microelectronics packages. A typical electronic package contains a single silicon chip, while a MCM contains multiple chips. In both cases the chip(s) are embedded in a protective substrate with metal leads protruding from the substrate to provide an electrical connection to the outside world (see Figure 1). Since the MCM contains multiple chips in one substrate, the chips can be packaged much closer together than if each chip had its own substrate. This close packing not only reduces the size of the electrical component, but it improves performance as well by shortening the length of the electrical leads, thus reducing the impedance of these leads and allowing high clock speeds.

On the MCM studied here, the chips are connected to each other through a High Density Interconnect layer or HDI for short. The HDI is typically made up of several layers of conducting materials that make up the signal, power and ground connections to the chips, separated by a

dielectric material, glued together by epoxies and connected by vias, as illustrated in Figure 2. The vias are the main focus of interest in this report.

It should be noted that there are several MCM configurations besides the one studied here. The configuration studied here is referred to as a "chips first design". It is different than typical MCM designs, in that typical designs create the interconnect layer first (not necessarily high density), and then attach the chip mechanically and electrically. The electrical connections are usually through wire bonds, tab bonds or solder bumps, while the mechanical connections are usually either through adhesives. For further information on the various types of MCM designs are presented in reference [1].

In a "chips first" design the chips are placed first, as the name implies, before the HDI layer is deposited. This design consists of a substrate with wells milled precisely to the depth of the silicon chips. These chips are then placed into the wells and held in place by adhesives, so that the top of the chip and substrate are flush. Finally each layer of the HDI is laid upon the chip and substrate, making electrical connections similar to the internal connections of a computer chip.

The chips first design is intended to be a high performance design aimed at very high end equipment such as mainframes or super computers. Currently, lower cost MCM designs are just entering the mass market place, as seen with Intel's next generation x86 CPU, the Pentium Pro (formally known as the P6), using MCM technology with two dies [2].

## **1.2 Via Reliability**

Typically several thousand vias reside within one MCM, and there may be several MCMs within one electronic device, such as a computer or radar guidance system. If one of these

thousands of vias should happen to fail, then it could potentially fail the entire system. Hence, the reliability of an individual via must be extremely high, or one must face the potentially costly alternative of building a large degree of redundancy into the MCM.

Several via failures have been observed during severe thermal cycle testing, and the cause of these failure must be understood. This report will concentrate on exploring the thermomechanical robustness of the GE via design.

### **1.3 The Analysis**

First we will examine the global stress/strain state of the entire MCM in order to understand the stresses (boundary conditions) placed upon the via. Then, using these boundary conditions, we will examine the stresses/strains within a single via. We will show that the model predicts the highest strain in the same area where failures have been observed. We will then show the impact of several parameters upon via stress. We will also show that the analysis correlates reasonably well with experimental data.

The primary analysis tool used throughout the research was finite element analysis, made available through the commercial code ANSYS™.

## 1.4 Objectives

In summary the objectives of this report are to:

- Understand the failure mode of vias within chips first MCMs.
- Determine methods to reduce likelihood of failure.
- Methodically verify the results of the analysis both by cross checking finite element models with each other and by comparing the results of the models with empirical data.

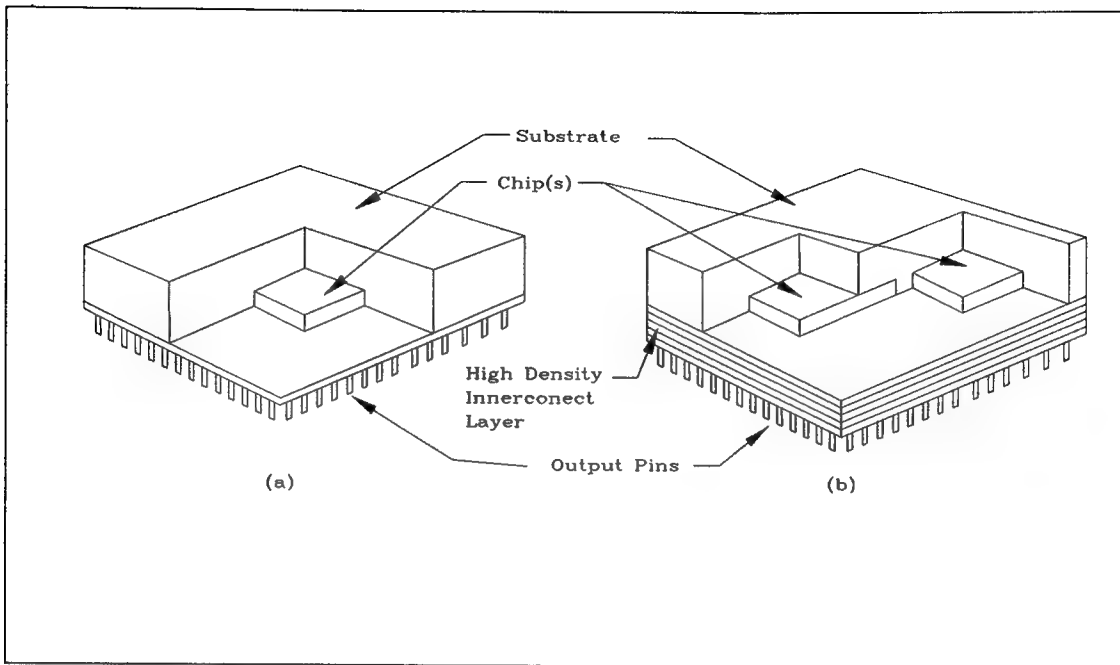


Figure 1. Schematic showing a cutaway view of (a) a typical electronic package (b) a multi-chip module (MCM). Note that drawing is not to scale.

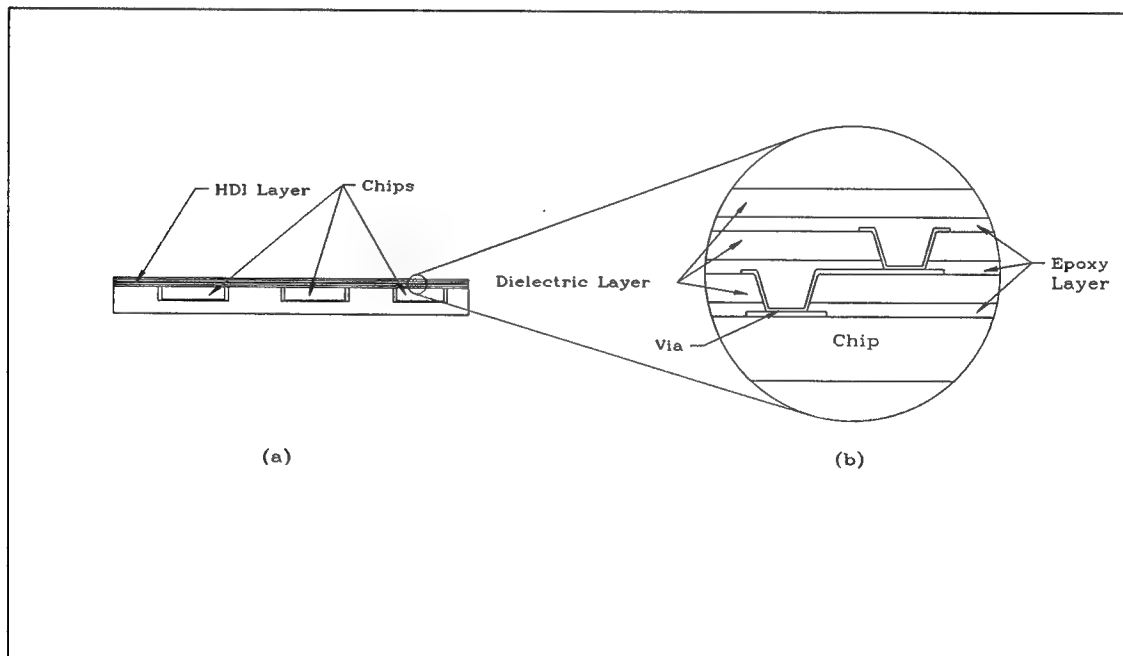


Figure 2. Schematic showing (a) the HDI layer within a MCM, and (b) a close up of the via structure within a MCM. Note that drawing is not to scale.



## CHAPTER 2

### RELATED WORK

In general when a product fails, it is for one of three reasons. Either the product did not meet the design specifications, the design specifications were inadequate for the product's intended use, or the product was not used as intended. Here we will examine two papers that relate to the first two causes of failure.

#### 2.1 Via Hole Failure Study, by A. Isobe *et al*

Work by Isobe *et al* [3] focuses on the failure of the bond between the via, and the via landing pad. In this mode of failure, the so called peeling stress created by the expansion of the dielectric layer overcomes the strength of the via/landing pad bond (Figure 3). Since the strength of the bond is proportional to the area of bond, and the peeling force is proportional to the circumference, this type of failure is most pronounced in small vias (less than 1.5  $\mu\text{m}$  hole width) with high circumference to area ratios.

Isobe *et al* found that the strength of the bond was related to the atomic concentration of fluorine between the via and the landing pad. The fluorine is deposited on to the via landing pad before the via creation as a by product of the via hole etching and cleaning. During via hole Reactive Ion Etching (RIE), the aluminum landing pad is sputtered, so that it is mixed with the fluorine

residue. The addition of aluminum makes the cleaning of the residue difficult since there is no solution that will etch the residue without etching the landing pad.

This residue layer has no noticeable impact on electrical resistance, making it difficult to detect. However it serves as a barrier to the bonding of the via to the landing pad. This weakens the bond and makes the via more prone to failure.

Isobe *et al* found that an etching technique known as the ECR - type system can reduce the failure rate significantly. In this system the etching ion energy can be lowered without lowering the etch rate. This prevents the sputtering of the via landing pad during the etch of the via hole, thus eliminating the mixing of aluminum with etching residue. Since the residue no longer contains any aluminum, it is much easier to remove, thus improving the strength of the via/landing pad bond.

Recall that this type failure is most dominate in vias with hole widths less than 1.5  $\mu\text{m}$ . Since the via we will be studying has a hole width ranging from 26 to 40  $\mu\text{m}$  and since no failures of this type have been observed, we do not expect this as a cause of failure.

## **2.2 A Thermo-Mechanical Fatigue Analysis of HDI Vias, by Prabhu *et al***

Work by Prabhu *et al* [4] attempts to determine the failure modes of vias using finite element analysis. In this paper several possible failure modes were examined:

- Thermal shock (transient analysis)
- Quasi steady state thermal cycling (fatigue)

In addition, the following effects were examined:

- orthotropic vs. isotropic material properties

- variation of the base material below the via (dielectric vs. chip)
- effect of sharp corner at the via-via pad interface

In their analysis they made the following assumptions:

- temperature and coefficient of thermal expansion (CTE) mismatch are the only causes of stress
- symmetry about the via center plane
- residual strains are zero at 23 °C
- zero x displacement at the left and right border of the model (the model lies in the xz plane with the z direction being through the thickness of the MCM)
- zero z displacement at the bottom of the model
- temperature range from -65 °C to 150 °C
- two-dimensional plain strain (equivalent to zero y displacement)

### 2.2.1 Thermal Shock (transient analysis)

The analysis showed negligible thermal gradients. This is due primarily to the large surface to volume ratio found on MCMs and to the extremely small dimensions of the via. Indeed, a temperature gradient of 25 °C/mm would be required to produce just a 1 °C differential across the via. Also, material studies conducted by Wu *et al* [5] showed that the temperature rate effect on the material properties to be negligible. From these two observations, we can conclude that quasi steady state conditions (uniform temperature) exist for an individual via, even under thermal shock conditions.

### 2.2.2 Quasi Steady State Thermal Cycling (fatigue)

At temperatures of 150 °C, stresses in the via barrel were approximately 190 MPa. Since a yield strength of 200 MPa was used, the analysis indicated that the via would not yield given a

defect free via. However, since some defects were expected, a strain concentration factor was introduced.

Given a circular notch in an infinitely wide material, the total concentration factor is 3.0 [6]. However with such a defect, yielding will occur. This yielding will cause the stress concentration to decrease and the strain concentration to increase. Neuber's rule was used to account for this, as follows:

$$K_t = \sqrt{K_\sigma K_\epsilon} \quad (1)$$

where  $K_t$  is the total concentration factor,  $K_\sigma$  and  $K_\epsilon$  are the stress and strain concentration factors respectively. Also a power law relationship was assumed for the constitutive equation of copper as follows:

$$\sigma = C\epsilon^n \quad (2)$$

where  $\sigma$  is stress,  $\epsilon$  is strain,  $C$  is a constant, and  $n$  is the power law exponent. Combining (1) and (2), using  $n=0.215$ , and using the definition of the stress concentration factor ( $\sigma=K_\sigma\sigma_o$ ), it was found that the strain concentration should be a maximum 8.6.

It should be noted that this stress concentration factor can only be considered a rough estimate. If such a defect was large compared to the via wall, then the assumption of an infinitely wide material would be violated and the concentration would be higher. If the defect was small relative to the via wall, then fracture mechanics would be more appropriate than stress concentrations.

Using the results of the analysis, and the assumed strain concentration factor, the Engelmaier model [7] was used to estimate the life of the via. This model relates strains to life for electrodeposited copper. The model is as follows:

$$\Delta\epsilon = N_f D_f^{0.75} - 0.9 \frac{S_u}{E} \left[ \frac{\exp(D_f)}{0.36} \right]^{0.1785 \log(10^5/N_f)} \quad (3)$$

where  $S_u$  is the tensile strength of the material,  $D_f$  is the fatigue ductility coefficient,  $E$  is the elastic modulus of the material, and  $N_f$  is the number of cycles to failure. The first term represents the contribution of elastic strain to life, while the second term represents contribution of plastic strain.

Assuming a ductility of 10% it was found that the life can range from 15 to 100 cycles for a strain concentration ranging from 3.0 to 8.6, given a  $\Delta T$  of 215 °C. For  $\Delta T$  of 165 °C and 40 °C the predicted life is 1000 and >100,000 cycles respectively. Note that a ductility of 30% yielded roughly a three times improvement in life as shown in Figure 4.

However we must again give a caution. In calculating their results, Prabhu *et al* used negative von Mises strains. Since the von Mises effective strain is not defined below zero, and since no further explanation was given, we cannot be sure of the implications of the results.

However, regardless of type of strain used, or the method used to model defects, it is apparent that defects and ductility have a dramatic effect upon life. Hence careful attention should be paid to produce defect free vias with high ductility.

### 2.2.3 Orthotropic vs. Isotropic Coefficient of Thermal Expansion

It was found that orthotropic CTE produced higher stresses than an isotropic CTE. This should be expected since the largest contribution to the effective strain in the via barrel is in the out-of-plane direction ( $z$  direction), and the out-of-plane CTE is higher than both the in-plane CTE or the bulk CTE. Hence it is recommended that orthotropic CTEs be used.

#### **2.2.4 Base Material Below the Via (Dielectric vs. Chip)**

It was found that the stresses are higher when there is a chip below the via pad (level 0) rather than a dielectric (level 1 or higher). Although the explanation for this phenomenon was not given in their paper, it was found that the chip restricted the expansion of the dielectric, so that more strain was forced into the via.

### **2.3 Chapter Summary**

The following conclusions can be drawn from previous research:

- In vias with hole diameters less than 1.5  $\mu\text{m}$  via/landing pad debonding is a significant cause of failure.
- The byproducts of etching, especially fluorine, can significantly decrease the via/landing pad bond strength.
- Typical reactive ion etching will sputter the aluminum, causing it to mix with the by products, making cleanup difficult.
- With ECR type etching, it is possible to etch without sputtering the aluminum. Thus by product cleanup is easier, and via/landing pad bond strength is improved.
- Thermal transient effects are unimportant given the dimensions and material properties present in the via under consideration, even under thermal shock conditions.
- Given a defect free via, the stresses approach yield at 150 °C. With assumed defects, the via can yield anywhere in the barrel section.
- Defects and fatigue ductility have a large impact on via life.
- Orthotropic coefficient of thermal expansion causes higher stresses than bulk properties.
- A stiff material, such as a chip, below the via increases the strains in the via by limiting the expansion of the epoxy and dielectric.

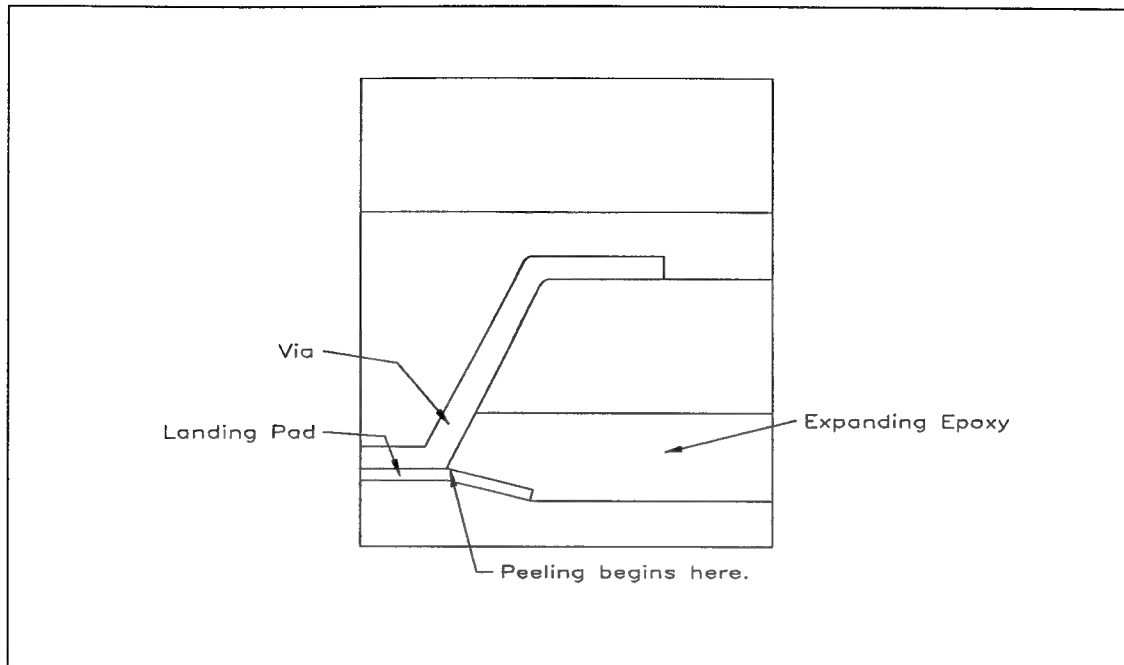


Figure 3. Schematic showing the via/landing pad peeling phenomenon reported by Isobe *et al* [3]. Note displacements are exaggerated.

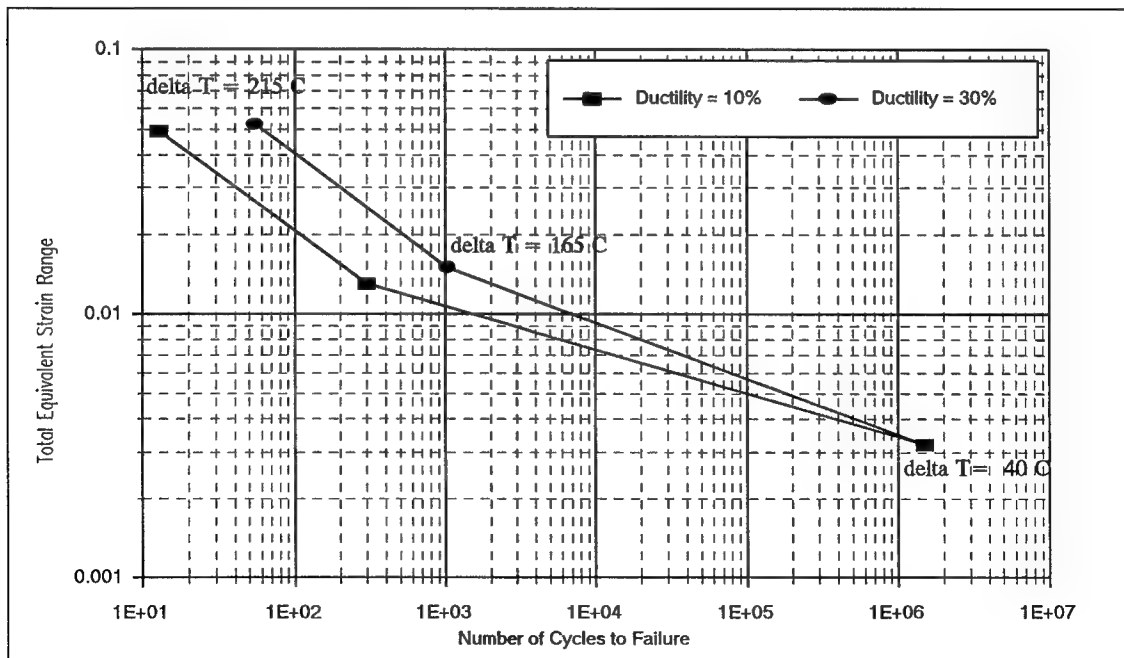


Figure 4. Life vs.  $\Delta T$  calculated with the Engelmaier model and a plane strain finite element analysis reported by Prabhu *et al* [4].

## CHAPTER 3

### GLOBAL ANALYSIS

In the present work, two finite element models and an analytical model were developed to understand the global stress/strain in the MCM:

1. A two-dimensional finite element model of a slice of a MCM (slice parallel to z axis).
2. A two-dimensional analytical model of a slice of a MCM using beam theory.
3. A three-dimensional finite element shell model of an entire MCM.

Model 1 allows us to look at a slice of a typical MCM in fine detail without a large runtime penalty (See Figure 5 for a schematic). However, this model can not take into account the effect of features out of the plane of the slice. Also, we must assume either plane strain or plane stress, and neither assumption may apply if state of stress in the MCM is indeed three dimensional.

Model 2 is essentially the same as model 1 except that it uses a relatively simple equation to predict the stress/strain field rather than a finite element model. This equation allows us to understand the impact of changing parameters on the global stress/strain field better than a finite element model. However, with this model we must make the assumption that planes remain plane, which is not strictly true due to coefficient of thermal expansion (CTE) mismatch.

Model 3 was created primarily to verify the assumptions of models 1 and 2. Since model 3 uses 16 layer shell elements (ANSYS element Shell 91), one element can be used to model the



entire thickness of the MCM (See Figure 6 for a schematic). Hence the entire MCM can be modeled with few elements, thus avoiding large penalties in CPU time, memory, etc. However, shell elements assume that vectors normal to the shell remain straight, and this is not strictly the case due to the CTE expansion mismatch.

None of the three models are ideal, each having disadvantages and assumptions. However, by using three models one can check the assumptions of one model with the other two and thus have a higher degree of confidence in the integrity of the results.

One should note that a three-dimensional brick mesh would have been the preferred model, since it would not be hampered by many of the two-dimensional, or shell assumptions. However, a model of sufficient detail would have required excessive amounts of computer resources. Hence a three-dimensional model was not pursued at this time.

### **3.1 Two-Dimensional Finite Element Model**

#### **3.1.1 Two-Dimensional Finite Element Model Assumptions**

The following assumptions are made explicitly or implicitly when creating this model:

1. Our material properties are accurate
2. The MCM has only rigid body constraints
3. Temperature is the only load
4. Temperature loading is spatially uniform
5. Residual stresses are zero at 23 °C
6. Geometry not on the "slice" have no impact on "in slice" stresses/strains
7. Plane Stress

8. The vias do not affect the global stress/strain state of either the MCM or the HDI

Assumption 1 is so implicit in any analysis that it is usually not mentioned. However, it is mentioned here because of the nature of the materials used. The HDI layer of the MCM is made up primarily of polymers, which are known to have non-linear material properties with wide batch to batch property variation. Also, since the dimensions of the HDI are so small, the material becomes orthotropic as well.

The rest of the assumptions are made primarily for simplicity purposes. Assumptions 2-5 are made because the true conditions would be difficult to obtain and would not be likely to yield any more information. If more specific boundary conditions were applied, such as a non-uniform temperature field, the information yielded would not be general in nature. While detailed boundary conditions may be useful for determining the modes of failure for a particular via, it would be difficult to extract general via design rules.

Assumption 6 is made to highlight an intrinsic fault of any two-dimensional analysis. The consequences of this assumption can be better understood after discussing the results of the two-dimensional model. Hence, more detailed discussion of this assumption is given in **Section 3.3**

### **Limitations of a Two-Dimensional Approach.**

Plane stress (assumption 7) was assumed in the model. However this assumption is almost irrelevant. Both plane strain and plane stress were modeled, and the stresses in the slice were nearly identical (the slice lays on the xz plane, where the z direction is through the thickness of the MCM). An explanation of this is given in **Section 3.2 Two-Dimensional Analytical Model**.

Note that the "out of slice" stresses (y direction) cannot be modeled correctly with either the plane strain or plane stress assumption. The stresses are not zero due to CTE mismatch, and the strains are not zero due to thermal expansion. Hence, neither the y stresses, nor any stresses derived from y stresses (such as von Mises stress) are presented here.

Assumption 8 allows us to ignore the vias in the global model. The reasons for doing this are intertwined with the reasons for doing a separate global and local analysis. Accounting for the via effects would cause a large computer resource penalty, even in a two-dimensional model. If we could model the via effects with a global model, then we would not need a local model.

### **3.1.2 Two-Dimensional Finite Element Model Geometry**

The relevant model dimensions and materials are shown in Figure 7. Note that only "large scale" features are modeled. The individual HDI layers are modeled, but the vias are not. The dimensions and materials were taken from a GE "Chips First" MCM [8]. For details on material properties, please refer to Appendix B.

### **3.1.3 Two-Dimensional Finite Element Model Applied Load and Boundary Conditions**

This model was uniformly loaded to 100 °C with uniform temperatures. No other external loads were applied. Only rigid body displacement constraints were applied, so that the model would be allowed to expand freely. Figure 8 shows these boundary conditions.

### **3.1.4 Two-Dimensional Finite Element Model Element Plots**

Note that a user created macro insures that the worst aspect ratio is no greater than 18. While this ratio may appear high, the elements were rectilinear, no warnings were issued from ANSYS, and memory limitations precluded us from using a smaller ratio (there are already approximately

10,000 elements). The element plot is shown in Fig 9. However the high element density makes viewing the individual elements difficult.

### **3.1.5 Two-Dimensional Finite Element Model Discussion**

The purpose of this analysis is to understand the displacement field around a particular via so that the results can be applied to a fine scale local via model. Hence, displacements and strains are of primary interest with stresses being a secondary concern. Also note that the high aspect ratio of a typical MCM High Density Interconnect (~400:1) makes viewing typical stress plots impractical. Hence the results are displayed as graphs.

The graphs presented show the following:

1. x displacement variation through the thickness (z direction) of the HDI layer (Figure 10)
2. x strain (mechanical) through the thickness (z direction) of the HDI layer (Figure 11)
3. x strain (mechanical) through the length (x direction) of the HDI layer (Figure 12)

#### **3.1.5.1 X Displacement Variation with Z**

Data of  $u_x$  vs.  $z$  is taken at three locations: 1) at the left edge of the model, 2) in an area that contains a chip, and 3) in an area that doesn't contain a chip. In each area the data taken in the HDI layer alone. HDI layer consists of three layers of dielectrics (made of Kapton) glued to each other by two layers of epoxies (made of SPI EPOXY) as shown in Figure 7.

The data is shown in Figure 10. Examining this data we note that planes appear to remain plane (the lines remain straight) at all locations, throughout the thickness of the HDI except at the left edge of the model. In fact, a regression analysis shows that the correlation coefficient for a

plane (linear) fit of the data has a magnitude of no less than 0.999999. Hence planes remain plane away from edges.

Near the edges there is no extra material to constrain a plane to remain plane. However, examining Figure 10. we see that there is only a small deviation from a perfect plane, as shown by the non-straight line. Hence planes effectively remain plane at edges, with only minor error.

#### **3.1.5.2 X Strain Variation with Z**

Again data is collected in a chip area, in an area that doesn't contain a chip and at the left edge of the model, throughout the thickness of the HDI. The high plateaus in Figure 11 represent the strain in the dielectric layers and the low plateaus represents the epoxy layer strains. It can be seen that the strain in the dielectric layers effectively remains constant within a layer and from layer to layer in the two locations that are away from edges. Near the edges, the strains deviate only slightly from a constant value. The same phenomenon occurs in the epoxy layers.

In comparing the data from the three different locations, we see that the entire HDI is in compression. The compression is caused by the high stiffness and low thermal expansion of the substrate material (alumina). The package material does not expand as much as the HDI, thus constraining the HDI to be in compression.

The least compression occurs at the edges of the MCM since there is very little material to constrain the part. The most compression occurs in the area of a chip, due to the very low coefficient of thermal expansion of the chip (Si). Also the thermal coefficient mismatch causes significant bending in the area of the chip, which places even more compression on the HDI layer.

### 3.1.5.3 X Strain Variation with X

Next we examine the x strain vs. x graph at two locations: the top and the bottom of the HDI (Figure 12). Examining this plot, we see that the strain is nearly constant away from boundaries. In the area of a chip the compressive strain is higher than in an area without a chip (as seen in the other plots). Also the x strain goes to zero at the left and right edges of the model, as expected.

At the boundaries between chip and no chip regions, we notice a spike (actually a dip in magnitude) where the strain begins to approach zero. This spike is due to the 0.1 mm air gap between two regions. In this area the alumina package material cannot constrain the HDI layer and the magnitude of the strain is relatively low.

Before we proceed, we should define "away from boundaries". It appears from the analysis that planes remain plane, and strains are constant at least 2 mm away from the MCM edge or the chip/no chip interface. However, it is suspected that a finer mesh density will reveal an even smaller transition region.

Examining all of the plots we also note that the magnitude of the strain is not very high. In the HDI layer the magnitude of the strain never rises above 0.002. Since none of the materials exhibit significant plasticity until at least 0.010 strain, one can conclude that a linear analysis could have been performed, even with much higher temperatures. In fact an analysis was performed at 350 °C (with assumptions about the SPI epoxy material properties, since we only have data to 120 °C) that showed that the material still behaved linearly. Since the MCM is never expected to get that hot, the linear assumption is valid when considering global stress/strains.

### **3.1.6 Two-Dimensional Finite Element Model Summary**

In summary we have four important results:

- Planes remain plane away from boundaries.
- The strain remains constant within a chip or no chip region for a given HDI layer away from boundaries.
- The strain is nearly constant through the thickness of the HDI layer for a given material.
- The material remains linear.

These results have the consequence that a two-dimensional slice of the MCM can be modeled accurately with linear beam theory. Also, since the strains are constant away from the boundaries, we need not model an entire slice of the MCM. Instead, a small model could be created to further study the effect of the transition region. However the GE design specifications require that there be a via free "moat" around the chip boundaries. One can speculate that the moat was created for the very reason that it is difficult to determine the environment near boundaries. Regardless, since vias are not located near the transition regions they are not generally of interest.

### **3.2 Two-Dimensional Analytical Model**

This section will describe and show the implications of the analytical model. Please refer to Appendix C for a formal derivation of the model.

#### **3.2.1 Analytical Model Assumptions**

The following list of assumptions were made during the creation of this model.

1. Our material properties are accurate
2. The MCM has only rigid body constraints, so that it may expand freely
3. Temperature is the only load

4. Temperature loading is spatially uniform
5. Geometry not on the "slice" have no impact on "in slice" stresses/strains
6. Plane stress
7. Residual stresses are zero at given reference temperature
8. The vias do not affect the global stress/strain state of either the MCM or the HDI
9. Linear material properties
10. Plane sections remain plane

These assumptions are nearly identical to those for the two-dimensional plane stress finite element model. The only exceptions are assumptions 9 and 10. Both assumptions were made for simplicity purposes, and both were shown to be valid in the two-dimensional finite element model.

### 3.2.2 The Analytical Model

Since we assumed that temperature was the only load, then the sum of the forces and moments internal to the MCM must equal zero ( $\Sigma F = \Sigma M = 0$ ). This fact along with the other assumptions were used to create the analytical model as follows:

$$\epsilon_{el} = (\alpha(z)_{tot} - \alpha_i)\Delta T \quad (4)$$

where,  $\epsilon_{el}$  is the elastic strain,  $\alpha_{tot}$  is the total effective thermal expansion coefficient (function of  $z$ ),  $\alpha_i$  is the coefficient of thermal expansion for layer  $i$  (material property),  $\Delta T$  is the change in temperature from strain free temperature.

Note that  $\alpha_{tot}\Delta T$ , and  $\alpha\Delta T$  are the total strain, and the free expansion thermal strain respectively.  $\alpha_{tot}$  is given by:

$$\alpha_{tot} = \frac{\sum E_i h_i \alpha_i \bar{z}_i}{\sum E_i h_i \left( \frac{h_i^2}{12} + \bar{z}_i^2 \right)} z + \frac{\sum E_i h_i \alpha_i}{\sum E_i h_i} \quad (5)$$



where,  $E_i$  is the Young's Modulus for layer  $i$ ,  $h_i$  is the thickness of layer  $i$ ,  $\bar{z}_i$  is the distance of centroid of layer  $i$  from neutral axis,  $z$  is the distance of point of interest from neutral axis.

The first term in the right hand side of Eq. 5. represents the expansion coefficient due to bending. The second term represents the expansion coefficient of the neutral axis (or the average expansion). Thus we can say that  $\alpha_{tot} = \alpha_b + \alpha_n$ .

Note that the equations shown are for plane stress. For plane strain replace  $E_i$  with  $E_i/(1-\nu_i^2)$ , where  $\nu_i$  is the Poisson's ratio of the layer of interest. However, the effect of this term is minimal. Since Poisson's ratio does not tend to change much from layer to layer, the  $(1-\nu_i^2)$  factor will tend to cancel out in both terms of Eq. 5. Therefore the plane strain and plane stress results do not significantly differ.

### 3.2.3 Analytical Model Discussion

In general the model agrees with the FEA results within three significant figures (0.1%) at points away from the edge and away from the chip/package interface. Some of the results are shown in Table 1 at 100 °C. The components of the analytical elastic CTE is shown in Table 2 at several locations.

As Table 2 shows,  $\alpha_i$  and  $\alpha_n$  are constant throughout the thickness of the HDI layer for a given material, while  $\alpha_b$  varies with  $z$ . Also the  $\alpha_b$  can be neglected with little error in the area not over a chip, since it is small relative to the other expansions. In fact, it can be shown that the substrate material (alumina) dominates the expansion in this region, so that the total strain in the layer of interest  $i$  is simply  $(\alpha_{alumina})\Delta T$  with little error (<1%).

These results make sense intuitively when one considers that the stiffness of the HDI layer is much less than the stiffness of the alumina layer, so that the alumina should dominate in an area with no chip. In the area of a chip, the chip stiffness is significant compared with the alumina layer. This creates bending stresses that are significant and that cannot be ignored.

Fortunately, when we add the bending CTE to the neutral axis CTE, we find that the total CTE is small compared with free expansion CTE of any of the materials used. Hence in the area over a chip, we may assume the total strain to be zero. Simply put, the large compressive elastic strain cancels out the large tensile thermal strain, giving a total strain close to zero. This assumption will cause an error in the elastic strain of about 7 %.

#### 3.2.4 Analytical Model Summary

The following conclusions can be drawn from the analytical model:

- The results match the two-dimensional finite element model to three significant figures (0.1 %).
- The analytical model can be used in place of the two-dimensional finite element model.
- The total x strain of the HDI layer within the no chip region can be approximated by  $\alpha_{\text{alumina}}\Delta T$  with an error in strain of about 1% when compared to the two-dimensional finite element model.
- The total x strain of the HDI layer within a chip region can be approximated by zero with an error in mechanical strain of about 7% when compared to the full two-dimensional model.

The last two conclusions together will be referred to as the simplified two-dimensional model.

### **3.3 Limitations of a Two-Dimensional Approach**

The FEA and analytical results agree so well that it is unfortunate that real world MCMs are not two-dimensional. In a real world MCM the package will extend past the chip, as seen in Figure 13. This will give the MCM more resistance to bending in the area of a chip than shown in the two-dimensional model. This should lower the strains in the chip area, and increase the strains in the no chip area. Hence the two-dimensional model should provide bounds to the actual strains.

This limitation of the two-dimensional model prompted the creation of the shell finite element model to explore this issue further.

### **3.4 Shell Model Finite Element Analysis**

The primary reason for the development of the shell model is to verify assumption 8 of the two-dimensional plane stress model: that "out-of-slice" geometry has no impact on "in-slice" strains. With that in mind, we will not go into the same depth in this model as we did in the two-dimensional plane stress model.

#### **3.4.1 Shell Model Assumptions**

The following assumptions were made explicitly or implicitly when creating this model:

1. Our material properties are accurate
2. The MCM has only rigid body constraints
3. Thermal strains are the only loads
4. Temperature loading is spatially uniform
5. Residual stresses are zero at 23 °C

6. Vectors normal to the shell surface remain straight
7. The air gaps between the chips, and the substrate do not affect the global stress/strain state of either the MCM or the HDI layer
8. The vias do not affect the global stress/strain state of either the MCM or the HDI layer
9. Linear material properties

This set of assumptions are virtually identical for to the assumptions made for the two-dimensional plane stress model. The only differences are as follows:

- a. We assume normal vectors remain straight. This is essentially the same as plane sections remain plane, although it's extended from beam theory to shell theory. The two-dimensional plane stress model showed that planes remain plane away from boundaries. Hence it is reasonable to assume that normal vectors remain straight away from boundaries.
- b. We neglect the air gap around the chips. We are forced to make this assumption since the shell elements used (16 layer ANSYS Shell 91) does not allow zero stiffness layers.
- c. We assume linear material properties. The two-dimensional plane stress model showed that this assumption was valid.

### **3.4.2 Shell Model Geometry**

The geometry information was taken from the same GE "Chips First" MCM as in the two-dimensional plane stress model. Note that only "large scale" features are modeled. The individual HDI layers are modeled, but the vias are not. A scale schematic is shown in Figure 14.

### **3.4.3 Shell Model Element Plot with Boundary Conditions**

The applied boundary conditions are shown on the element plot in Figure 15. The model was loaded to 120 °C and only rigid body constraints are applied. A user defined program was defined to ensure that the maximum aspect ratio was no greater than seven.

#### 3.4.4 Shell Model Discussion

The primary reason for the creation of this model was to verify the assumption of the two-dimensional model that "out of slice" geometry has no impact on "in slice" strains. Realistically, we would expect the results of the two-dimensional plane stress model to bound the strains seen in the shell model, so that the predicted chip strain is an upper bound, and the predicted no chip strain is a lower bound of elastic strain magnitude.

However, the two-dimensional model only made predictions about the x strain. It says nothing about the y strain, unless we recognize that the chosen direction of the x axis was arbitrary. If we had chosen the x axis to be rotated 90° the results would be identical since the strains were constant within a chip or no chip area. Hence we might conclude that the y strain equals the x strain at any given point.

Upon examining the results of the shell model we find that it is better to conclude that the predicted x strains from the two-dimensional model are actually the average strains in the XY plane. We can show this by examining the z strain, since it is a function of the average XY strain. For a derivation of this function see Appendix D. See Figure 16 for a comparison of the predicted and actual z strain in the HDI layer of the MCM.

As can be seen, the two-dimensional model provided reasonably good bounds to the z strains and hence the average x and y strain, as expected. The simplified two-dimensional model is just as accurate a lower bound in no chip regions, and is almost as accurate upper bound in chip regions with thicker chips.

Hence, using the simple model to estimate the appropriate XY constraints in a chip area will overestimate the strains by 15-30% when compared to shell model data, depending upon the chip thickness. Since our goal is to determine failure modes of the via, and the simple model overestimates strain, it is conservative. Considering the simplicity of the simple two-dimensional model, the uncertainty in the other modeling assumptions, and the conservative nature of the model, the simple two-dimensional model becomes the model of choice for creating conditions for the local via model.

### 3.5 Application to a Three-Dimensional Local Model

As mentioned in the previous section, the results of the two-dimensional analysis can be considered bounds to a three-dimensional local analysis. Since the boundary conditions of a finite element analysis are usually only displacements and forces, we must convert our strain results into either displacements or forces. Since either is acceptable, and the former is easier, we shall convert the strains into displacements. The following assumptions are used:

- The bounding strains are given by the two-dimensional analytical analysis
- The strains in the XY plane are independent of direction
- No applied stress in the out-of-plane direction
- Quarter symmetry

Since the in-plane strains are assumed independent of direction, then the in-plane displacements are simply given by:

$$u_j = \epsilon_{tot} \cdot L_j = \alpha_{tot} \Delta T \cdot L_j \quad (6)$$

where  $L_j$  is the length of submodel in the j direction,  $\alpha_{tot}$  is given by Eq. 4

Note that the  $\Delta T$ , and  $\alpha$  of the finite element model must match that of the analytical model. Also,  $\alpha_{\text{tot}}$  will be a function of temperature if the material properties are a function of temperature. Hence, it may be necessary to calculate  $\alpha_{\text{tot}}$  for each  $\Delta T$  analyzed in a general analysis. However this is not necessary for this analysis, since the silicon and alumina dominate the expansion and these materials have temperature stable material properties.

No constraints are applied in the out-of-plane direction (z direction), other than to prevent rigid body motion. See Figure 17 for a schematic of the suggested boundary conditions.

As mentioned before, in the case of the MCM studied we may use of the simplified analytical model rather than the full analytical model (Eq. 4 ).The simple model states that  $\alpha_{\text{tot}} = 0$  in a chip area, and  $\alpha_{\text{tot}} = \alpha_{\text{alumina}}$  in a no chip area. This should yield less than 5% additional error in structural strains (elastic + plastic) in a chip area (for thick chips) and less than 1% additional error in a no chip area when compared to the full analytical model.

### 3.6 Chapter Summary

The following results were concluded from the two-dimensional finite element model, the analytical model, and the shell model.

- We can assume that plane sections remain plane away from boundaries for a two-dimensional analysis, and vectors normal to the MCM remain straight in a three-dimensional analysis, even though neither is strictly true due to thermal expansion.
- The structural strain is nearly constant through the thickness of the HDI layer for a given material.
- On a global scale, the material remains linear.
- The results of the analytical and finite element two-dimensional analysis correlate to three significant figures (0.1 %).

- The analytical model can be used in place of the two-dimensional finite element model. Hence, we will no longer attempt to distinguish the results of the two models.
- The results of the simplified analytical model correlate to the other two-dimensional models within 1% in a no chip region, and 5% in a "thick" chip region.
- The two-dimensional analyses predicts the bounding average strain in the XY plane with less than 1% error in the no chip region, and less than 10% error in the chip region.
- The bounding strains provides a conservative approximation for the entire strain range.
- The bounding strains from the simplified two-dimensional analysis can be used to compute displacement boundary conditions that are applied to a finite element submodel of a HDI via. This means that a full three-dimensional nonlinear finite element analysis of the entire MCM package is not required in order to obtain the appropriate boundary conditions for a finite element submodel of an HDI via.



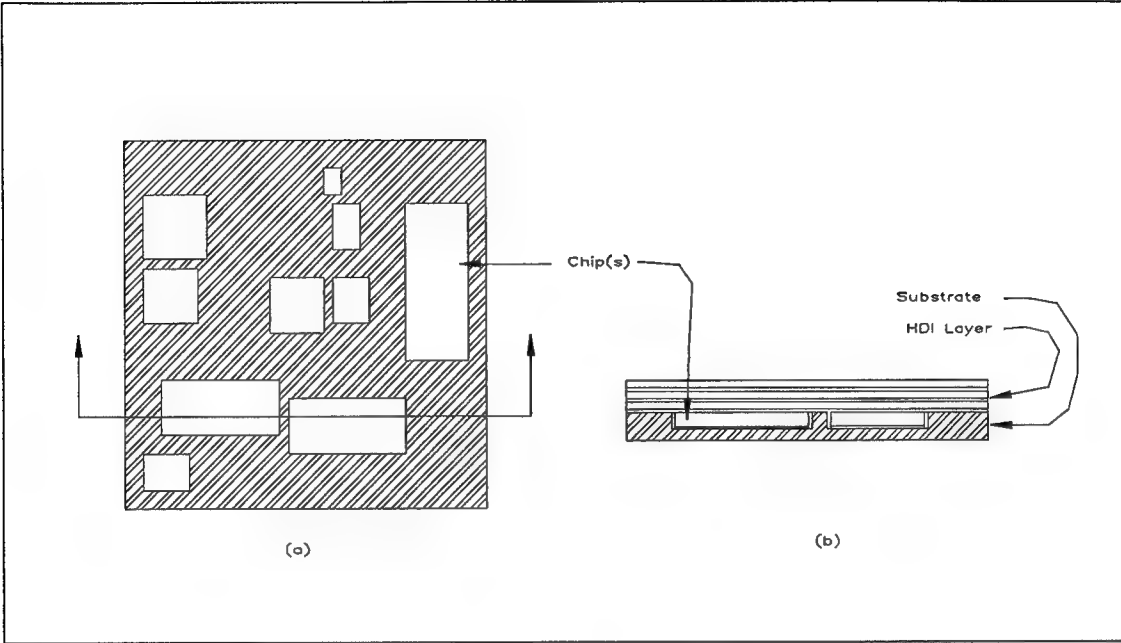


Figure 5. Location of "slice" for the two-dimensional finite element model of the MCM. (a) shows the "slice" location and (b) shows the cross section of the slice. The model is based upon on the GE "chips first" MCM design.

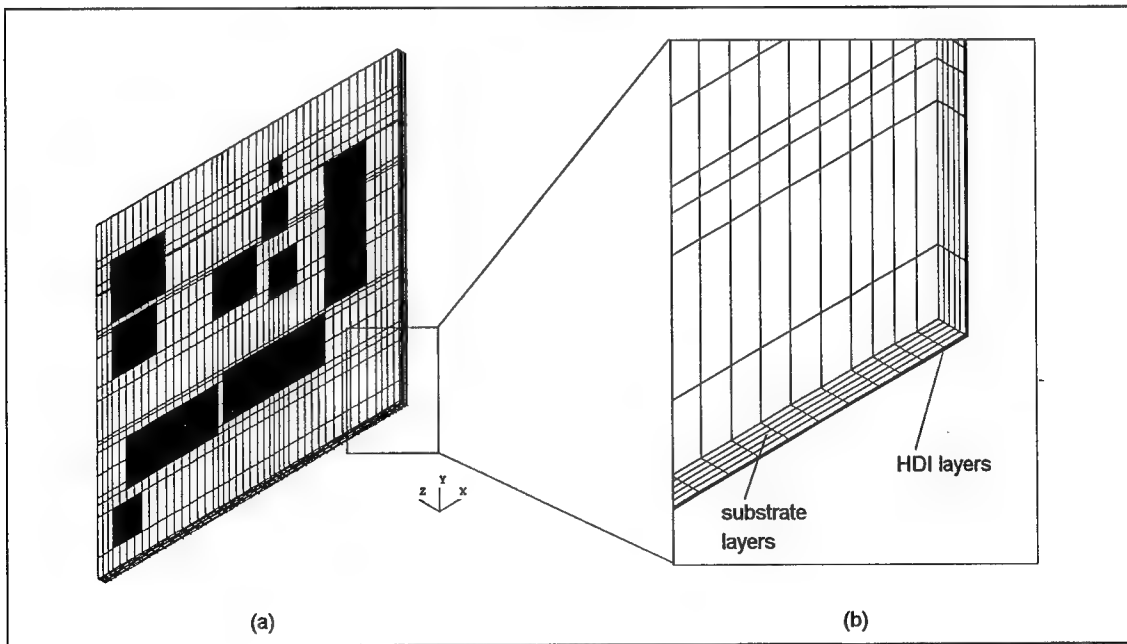


Figure 6. Shell model schematic. The ANSYS element Shell 91 allows up to 16 layers through the thickness of the element. This allows us to assign each layer of the MCM to a layer of the shell, so that one element can model the entire thickness of MCM. (a) shows a schematic of the mesh used in the shell model. (b) shows a close up of the layers of the shell.

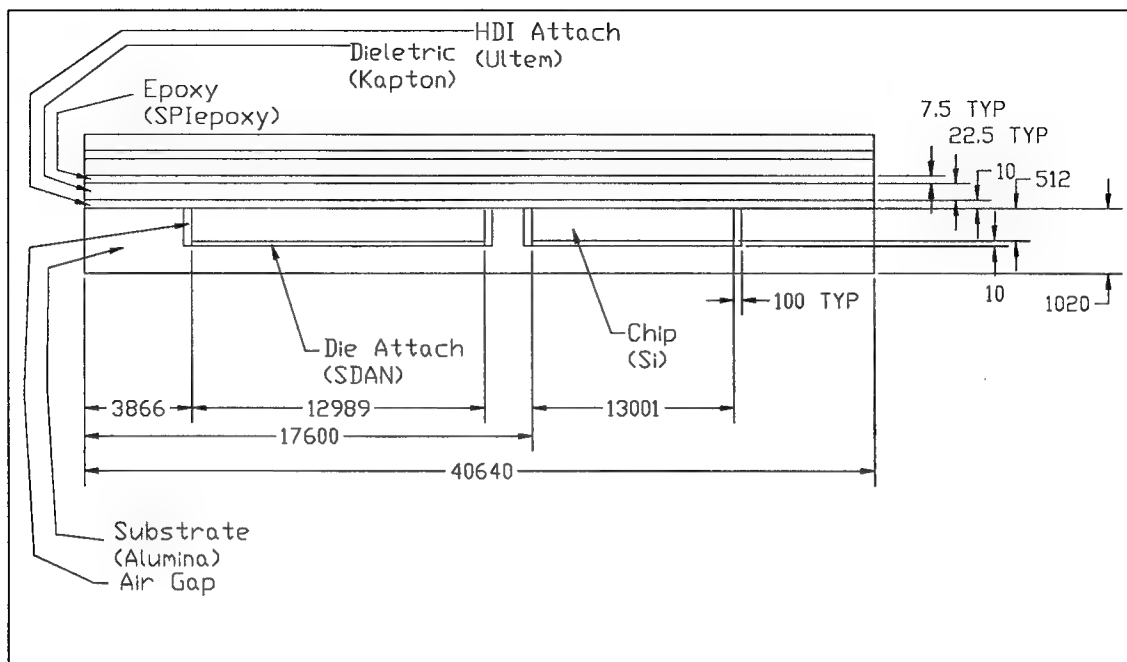


Figure 7. Model geometry for the two-dimensional finite element model. Note the schematic is not to scale and dimensions are in  $\mu\text{m}$ .

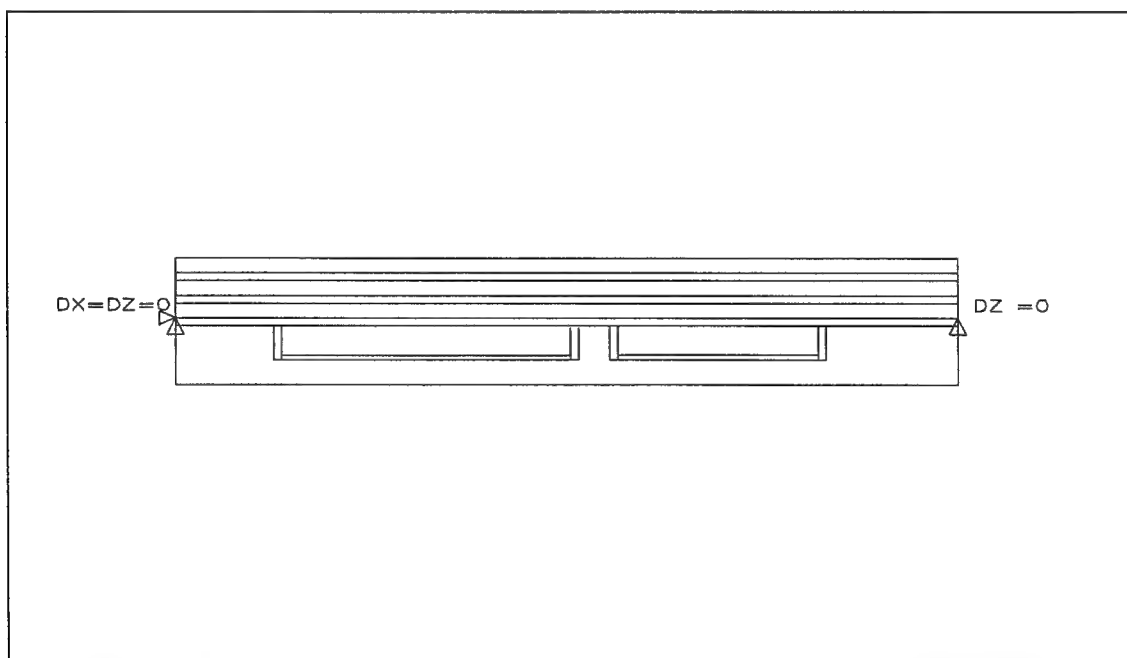


Figure 8. Boundary conditions for the two-dimensional plane strain finite element model. Note that the boundary conditions only prevent rigid body motion. A uniform temperature load of  $100\text{ }^{\circ}\text{C}$  was applied.

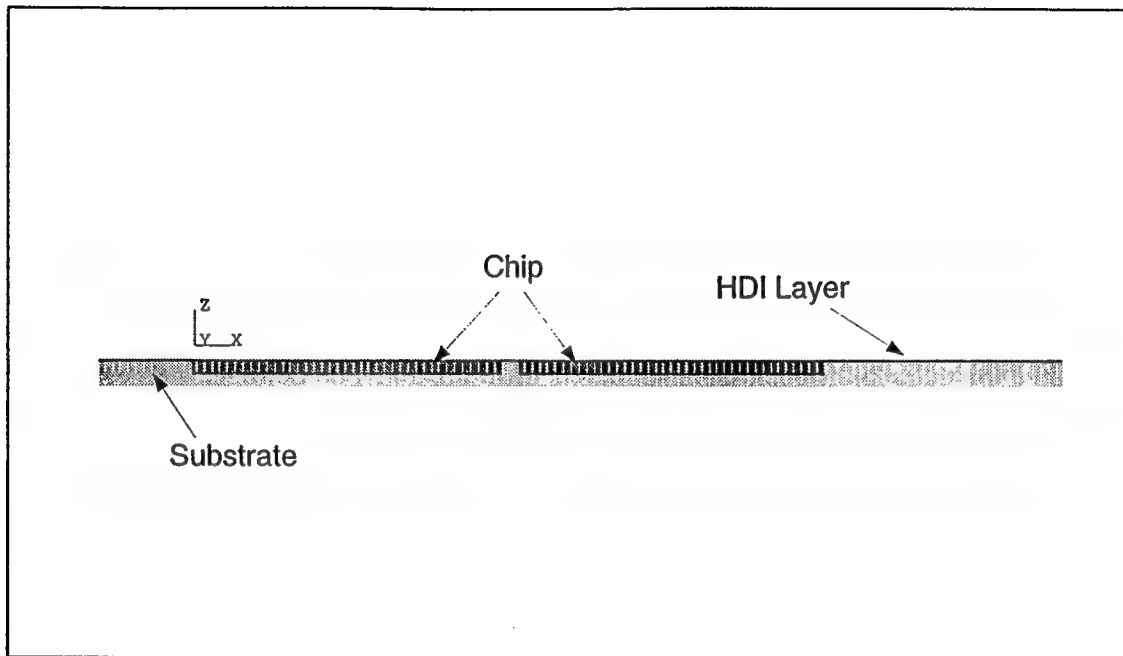


Figure 9. Element plot of the two-dimensional plane strain finite element model. Note that high element density makes viewing individual elements difficult.

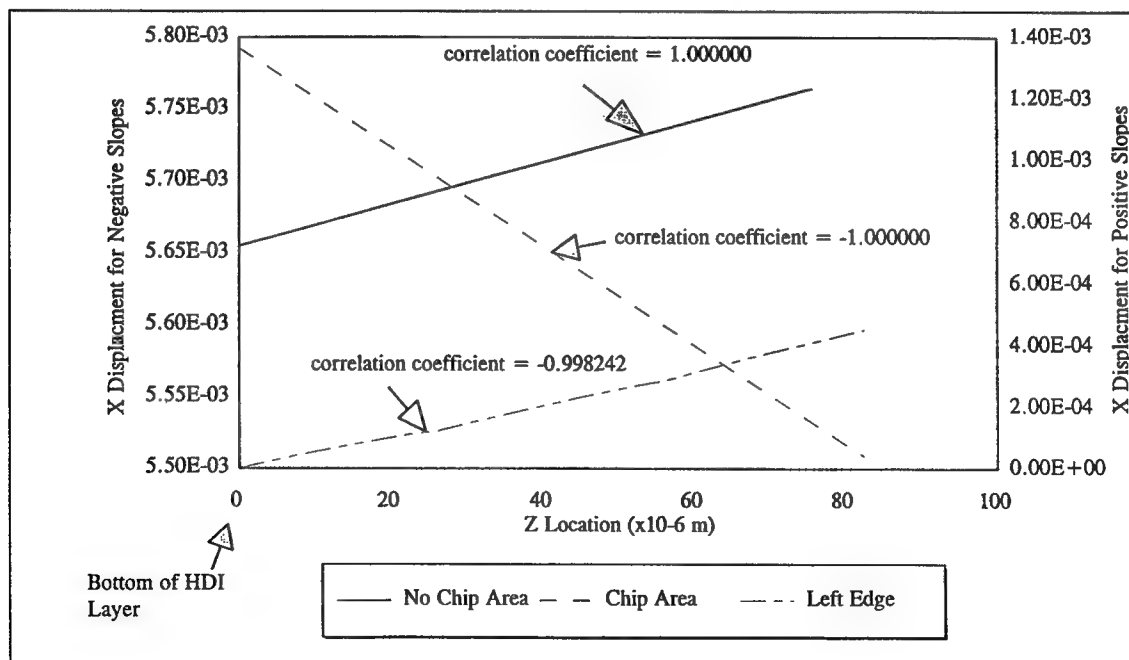


Figure 10. X Displacement vs. Z at 100 °C for the two-dimensional finite element MCM model. Note that magnitude of the slope is not important. It is only important that the lines remain straight, indicating that planes remain plane.

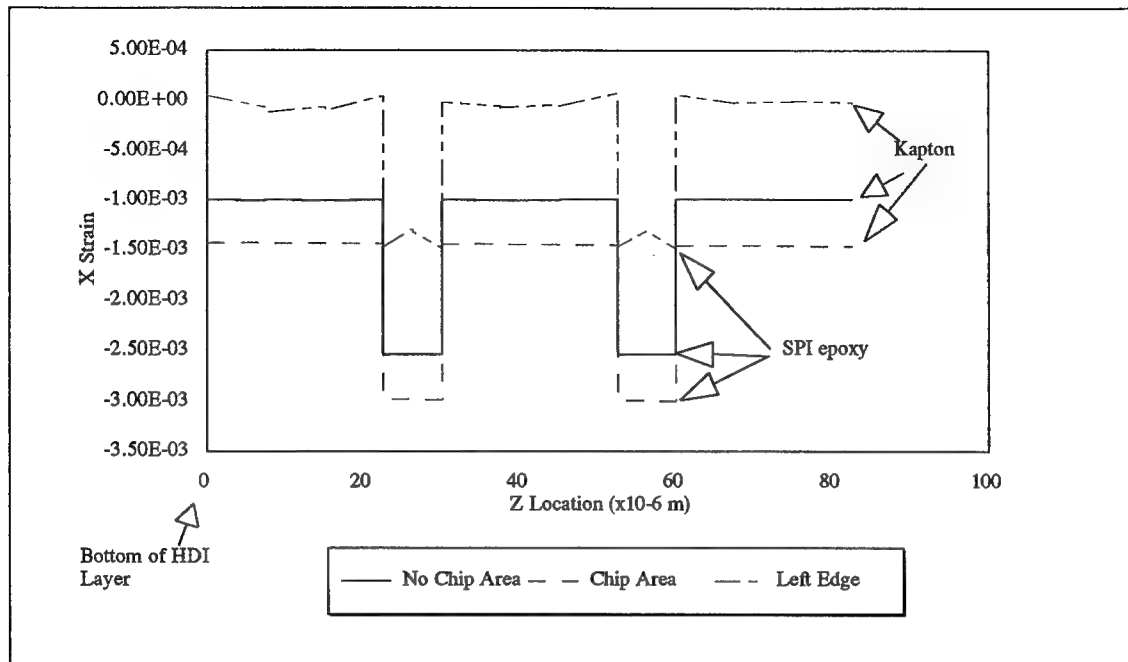


Figure 11. X Strain vs. Z at 100 °C for the two-dimensional finite element MCM model.

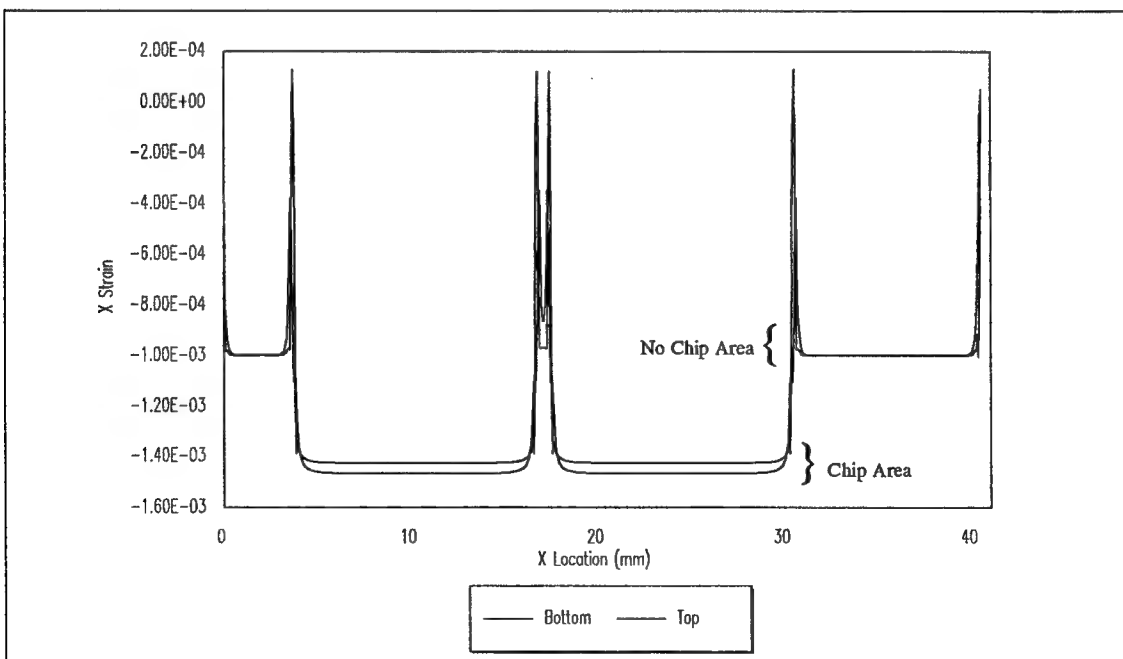


Figure 12. X Strain vs. X. At the top and bottom of the HDI layers at 100 °C. Note that the material is Kapton at both locations.

	Area Over Chip		Area Not Over Chip	
	$\epsilon_{el}$ Analytical ( $\times 10^{-3}$ )	$\epsilon_{el}$ FEM ( $\times 10^{-3}$ )	$\epsilon_{el}$ Analytical ( $\times 10^{-3}$ )	$\epsilon_{el}$ FEM ( $\times 10^{-3}$ )
Top of HDI	-1.46	-1.46	-0.995	-0.995
Bottom of HDI	-1.42	-1.42	-0.996	-0.996

Table 1. Comparison of the results of the two-dimensional analytical model with the two-dimensional finite element model.

	Area Over Chip			Area Not Over Chip			
	$\alpha_n$ ( $\times 10^{-6}/^{\circ}\text{C}$ )	$\alpha_b$ ( $\times 10^{-6}/^{\circ}\text{C}$ )	$\alpha_t$ ( $\times 10^{-6}/^{\circ}\text{C}$ )	$\alpha_n$ ( $\times 10^{-6}/^{\circ}\text{C}$ )	$\alpha_b$ ( $\times 10^{-6}/^{\circ}\text{C}$ )	$\alpha_t$ ( $\times 10^{-6}/^{\circ}\text{C}$ )	$\alpha_i^1$ ( $\times 10^{-6}/^{\circ}\text{C}$ )
Top of HDI	5.13	-4.09	1.04	7.02	0.06	6.96	20
Bottom of HDI	5.13	-3.7	1.43	7.02	0.05	6.97	20

<sup>1</sup> Value given is for Kapton.

Table 2. Components of the expansion coefficient derived from the two-dimensional analytical model.  $\alpha_n$  is the component of expansion due to the neutral axis growth,  $\alpha_b$  is the component of expansion due to bending and  $\alpha_t$  is the total expansion.  $\alpha_i$  is the CTE for layer

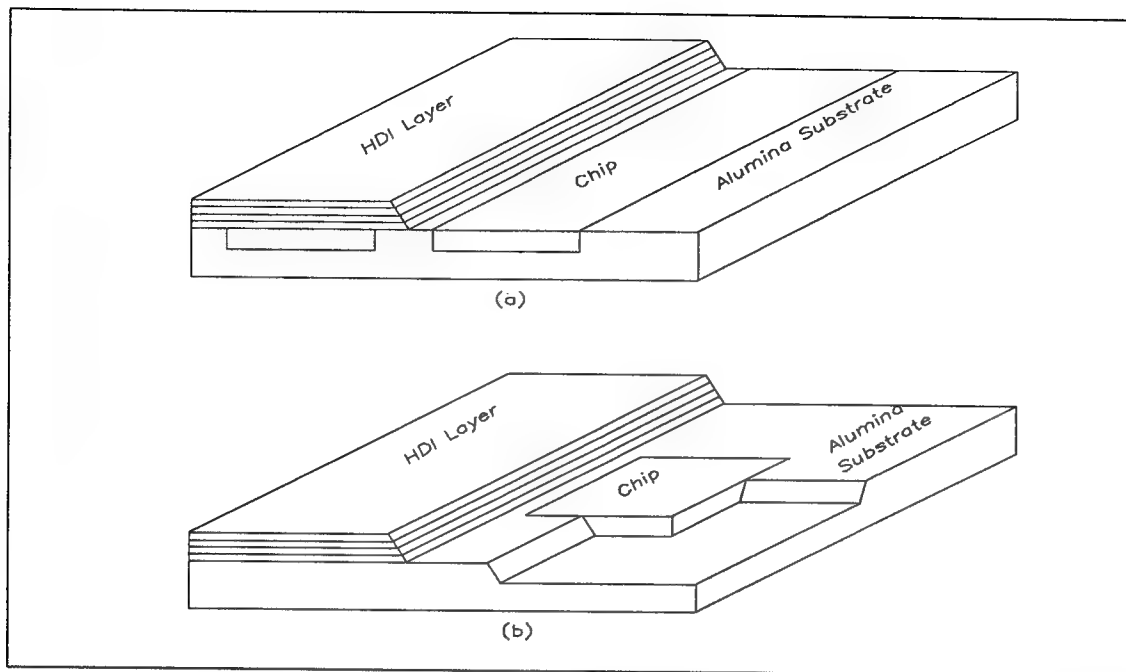


Figure 13. A cut away view of (a) a three-dimensional representation of the two-dimensional model, (b) a portion of an three-dimensional multi - chip module. Note, neither drawings are to scale.

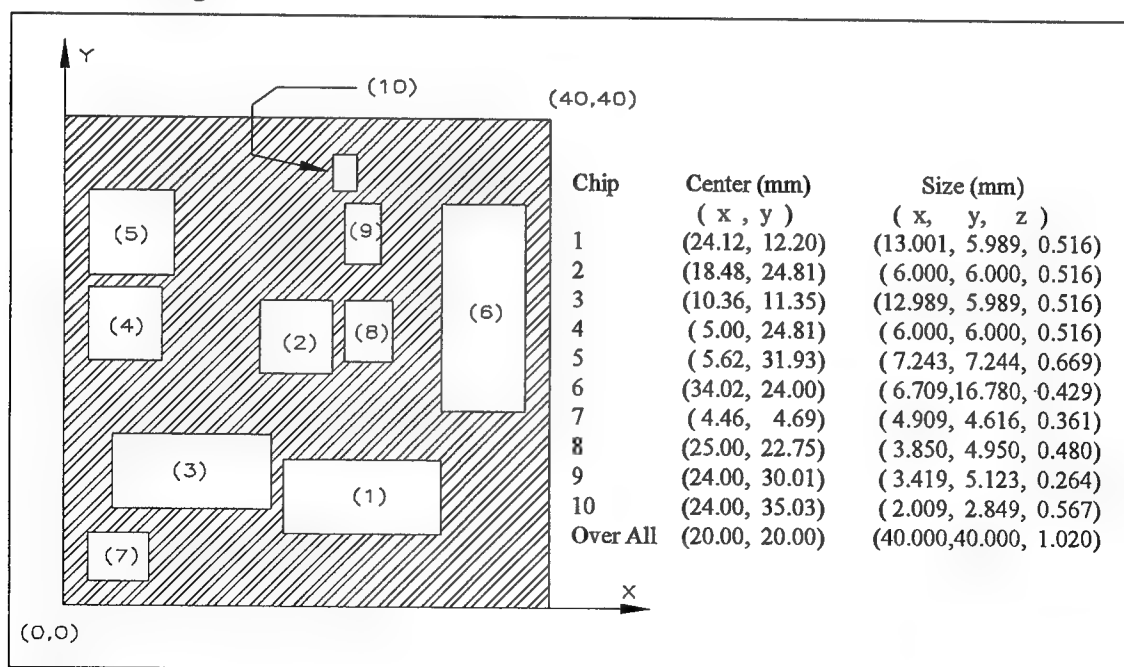


Figure 14. Geometry for the shell finite element model. Note that the chips are drawn for illustration purposes only. In reality the chips are completely embedded within the MCM so that they are not visible.

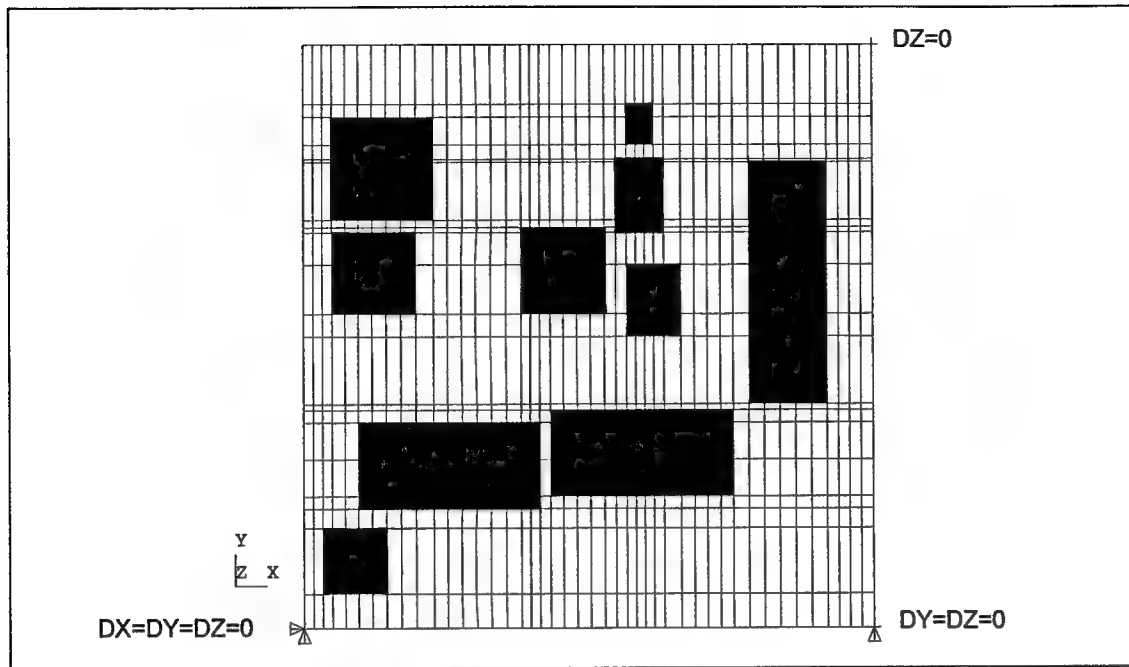


Figure 15. Shell model element plot with boundary conditions.

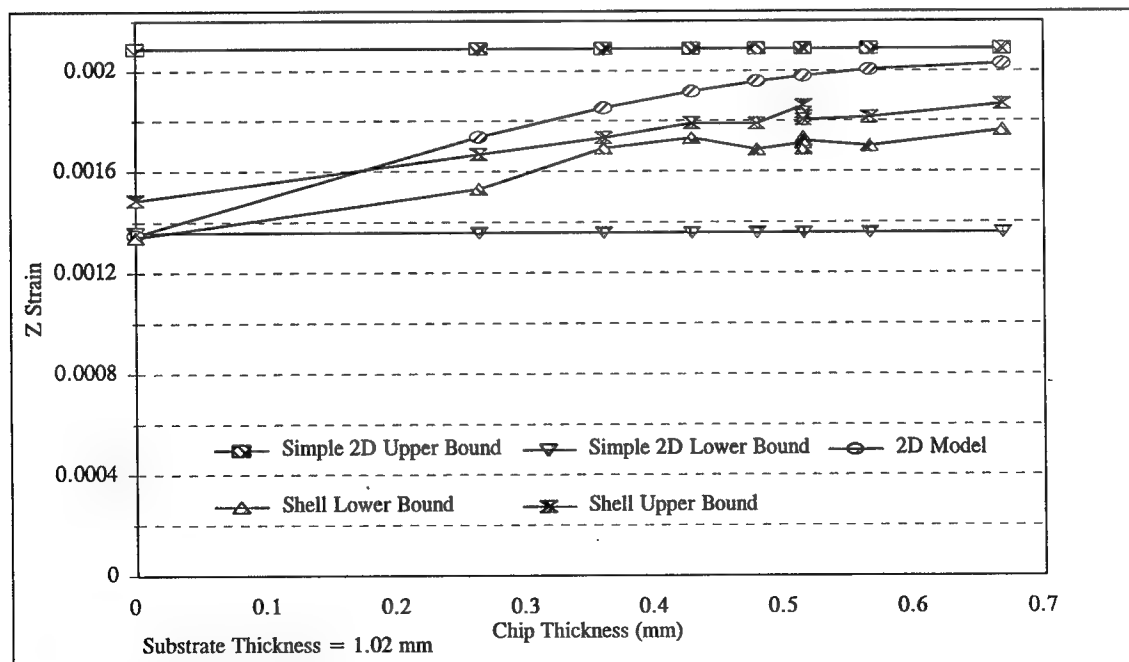


Figure 16. Z strain predicted from the two-dimensional model vs. the shell model. As predicted, the analytical model provides an upper bound, and a lower bound in a chip and no-chip area (chip thickness = 0) respectively.

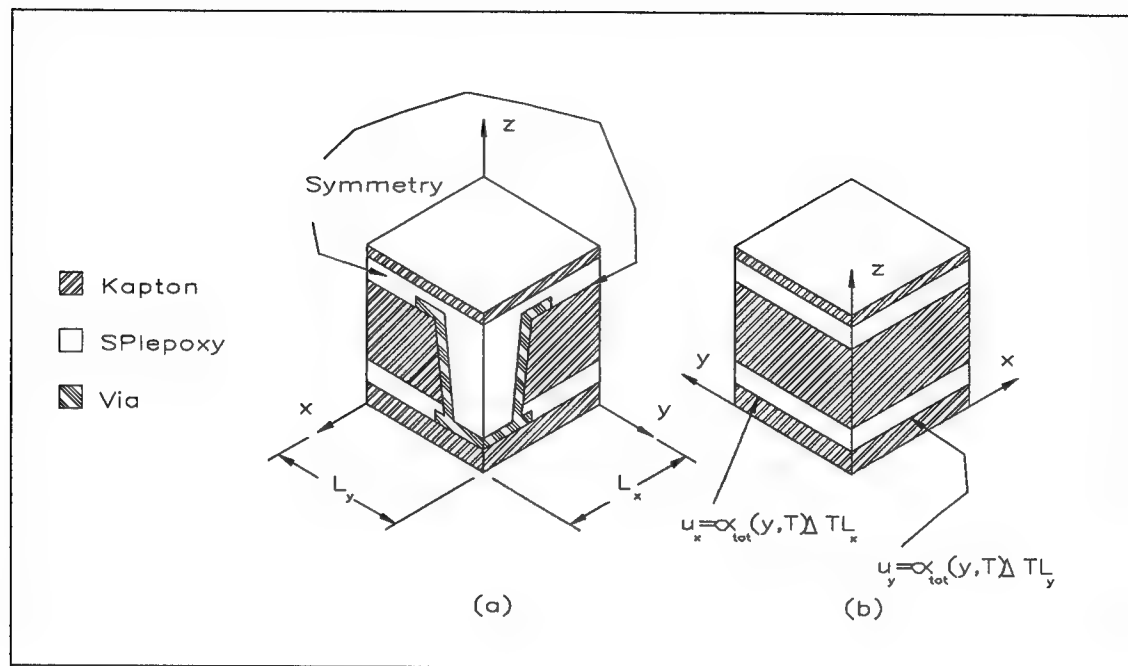


Figure 17. Suggested boundary conditions for a three-dimensional local analysis. (a) View showing the symmetry plane. (b) View showing the opposing planes.



## **CHAPTER 4**

### **LOCAL VIA MODELS**

Two families of local models were created to study the stress-strain state of a via. They are:

1. Two-Dimensional axisymmetrical finite element models
2. Three-Dimensional finite element models

The first model family was created because it is small and can be run quickly. This allows us to thoroughly explore the design space so that we can fully understand the state of stress and determine the causes of high stress.

The second model family should be more accurate, since it is a more realistic representation of the actual via geometry. However, the size of this model makes it very expensive in terms of run-time and disk space. Hence, model 2 will primarily verify the assumptions of model 1.

#### **4.1 Family of Axisymmetric Finite Element Models**

In order to understand the state of stress in the via, many different models were created with reference to one base model. In each model one parameter was changed so that we could observe the impact. In choosing the parameters, no restrictions were applied, so that any assumptions about dimensions, material properties, etc. may be tested. This approach allows us to determine which parameters are significant, so that we may fully understand the behavior of the via.

#### 4.1.1 Assumptions

The following assumptions are made explicitly or implicitly when creating the base model:

1. Our material properties are accurate
2. Temperature is the only load
3. Uniform temperature
4. Residual stresses are zero at 23 °C
5. Axisymmetric geometry
6. Total radial strain equals zero away from the via
7. Linear uniform material properties

Assumptions 1 through 4 are made for the same reasons as for the global model in **Chapter**

3. We assume an axisymmetric geometry for the base model because this is the best two-dimensional approximation for modeling the corners of the true rectilinear geometry. However, one might argue that the mid-points of the walls may be of more interest, so that a plane stress or strain assumption may be more appropriate. Hence, we created a plane stress and strain model and compared all three to a preliminary three-dimensional model to test this assumption.

Assumption 6 was justified from the conclusions in **Chapter 4** for chip areas. Non-chip areas were not seriously examined because preliminary analyses revealed that only level zero vias (vias that are directly attached to chips) are under any significant strain.

Assumption 7 states linear material properties. We assume this because linear models run very fast. This allows us to make many models to test many parameters. However, the actual nature of the local strains about the via are highly non-linear. Hence linear models can only be use

for comparison purposes. Actual values of strain will not be quantitatively accurate and are not given for any linear models. Note that a non-linear version of the base model was created to demonstrate that the linear model has the accurate qualitative results.

#### 4.1.2 Model Geometry and Parameter Map

A scale drawing of the geometry is shown in Figure 18. The dimensions and materials are shown as parameters since many different specific models were created.

Table 3 shows the actual dimensions, materials and other options for each model created. Each model in Table 3 is identical to the base model, except for one parameter. However several "special" models were created that changed more than one variable. They were created to illustrate a specific point. The models names and descriptions are :

1. LevOne Model: This model studies the state of stress on a level one via, or more accurately a non-level zero via (a via not attached directly to the chip). The differences are as follows: Silicon replaced by Kapton, Ultem replaced by SPI EPOXY, epox1hgt set equal to epox2hgt.
2. AllEpox Model: This model studies the effect of the Kapton/Ultem intermaterial boundary. It replaces the Ultem and Kapton with SPI EPOXY, so that there is no intermaterial boundary.
3. AlpIn Model: This model studies the effect of the in-plane (x and y dir.) CTE. It replaces the Kapton, SPI EPOXY and Ultem with a "custom" material with  $CTE_z = CTE_{Cu}$ ,  $CTE_{xy} = 5 * CTE_{Cu}$ ,  $E = E_{Cu}/10$  and  $\nu = \nu_{Cu}$ , with E and  $\nu$  being Young's modulus and Poisson's ratio respectively.
4. AlpOut Model: This model studies the effect of the out-of-plane (z dir.) CTE. It replaces the Kapton, SPI EPOXY and Ultem with a "custom" material with  $CTE_z = 5 * CTE_{Cu}$ ,  $CTE_{xy} = CTE_{Cu}$ ,  $E = E_{Cu}/10$  and  $\nu = \nu_{Cu}$ .

#### 5. Alptotx Model

This model was created to help justify assumption that the total radial strain is zero away from the via. The opposite extreme in this case would have the radial strain equal to that of alumina. Hence, the radial displacement is set to the expansion of alumina ( $\Delta u_{rad} = CTE_{alumina} * \Delta T * \text{model radius}$ ).

### 4.1.3 Boundary Conditions and Element Plot

The following are the constraints:

1. Completely constrained in the X (radial) direction
2. Rigid body constraints only in the Z (axial) direction
3. Reference temperature of 23 °C
4. Load Step 1: Uniform temperature of -65 °C
5. Load Step 2: Uniform temperature of 120 °C

The temperatures for load steps 1 and 2 were chosen in relation to a standardized via abuse test [9]. In this test an MCM is repeatedly cycled between -65 °C and 150 °C, under thermal shock conditions. Although one may expect significant temperature gradients to form, a study by Prabhu *et. al.* shows that the dimensions and materials of the MCM/via are such that a uniform temperature may be assumed. Unfortunately our material property data only goes to 120 °C, hence we cannot model the standard test at 150 °C. However, this makes little difference in the understanding of the via strain behavior. See Figure 19 for a schematic of the applied boundary conditions on the base model mesh.

### 4.1.4 Discussion

Experimentally, most failures have been observed on the level zero via (via failure location provided by GE, based upon in-house testing), just below the Kapton/Ultem interface. This is

where we expect to see failure in the finite element models. Indeed, the base model shows a strain concentration just below the Kapton/Ultem interface on the inside of the via wall. This concentration will be referred to as the primary concentration. However, this is not the highest strain in the linear model. There are two other concentrations that have strains approximately 30% higher. These other concentrations cover a small area compared to the primary concentration. Hence, we may expect yielding to relieve the other concentrations before the primary concentration. The non-linear analysis shows this to be true. Since the linear run correctly shows the location of the primary stress concentration, it can be used to compare relative values to determine trends. See Figure 20 for a comparison of the concentration in both the linear and non-linear models.

#### **4.1.4.1 Non-Linear Model**

Figure 21 shows the effective plastic strain in the via. Note that any non-zero strains indicate that yielding has occurred. Since the entire via wall has non-zero strains, then the entire via wall has yielded. Note that the entire via wall also yields at -65 °C. Since the standard thermal abuse test cycle between -65 °C and 150 °C, then the entire via wall is cycled through a hysteresis loop and low cycle failure is expected.

#### **4.1.4.2 Modes of Failure**

Figure 22 shows the effective linear structural strain along the inside via wall for various models. Note that the strains are much less in the plane strain and the level one axisymmetric

model, to the point where no yielding would occur. Also the stress concentration is eliminated in these models.

The lower strain of the level one vs. the level zero model can be understood by examining the displacement plot for both models (Figure 23). In the case of the level one via, the expanding Kapton layer is allowed to expand over the top and below the bottom of the via. However, the level zero via is attached to a stiff silicon layer, preventing the expansion of the Kapton below the via. Hence more strain is driven into the via.

Note that the effect here is somewhat exaggerated, since nothing is constraining the bottom of the bottom layer (silicon on a level zero via, and Kapton on a level one via). With such a constraint, the stress levels on a level one via would be somewhat higher. However, the trend is correct, and that is our primary concern here.

The lower strain of the plane strain model compared to the axisymmetric model is due to their decreased stiffness. The plane stress or strain assumptions effectively models the via wall as a sheet, so that it has very low stiffness in bending and thus accommodates significant deflection without much strain. The axisymmetric assumption adds curvature to the "sheet", thus stiffening it. However the loading is largely displacement driven, so that a stiffer via simply gives higher stresses, more yielding and therefore much higher strains.

Based upon the comparison of the axisymmetric and plane strain models, we would expect the strain concentration to appear predominantly in the corners of the three-dimensional via model, since the corners have the highest stiffness. Indeed, we will show this later in this chapter.

Again examining Figure 22, we see that the AllEpoxy model has a significant stress concentration. Recall that this model uses SPI epoxy for both the Ultem and Kapton. While the concentration is not as high as the base model, its mere existence is significant since there is no Kapton/Ultem intermaterial boundary in this model.

Previous investigators suspected that this intermaterial boundary may have been the cause for the failures. The failures occurred near the boundary and intermaterial boundaries have been known to produce stress singularities. However in this case we still have a stress concentration without the boundary. Hence the boundary is not responsible for the stress concentration and has little or nothing to do with the cause of failure for the via.

Again examining Figure 22, we see that the strains for Alphin model is significantly higher than for the Alphout model. This implies that a CTE in the in-plane (xy) direction is more significant than a CTE of the same magnitude in the out plane direction (XY). This surprising result is due to the fact that the model is not allowed to expand radially, thus forcing a large Poisson expansion in the z direction. With the radial displacement set equal to zero, and with Poisson's ratio greater than 1/3 it can be shown that the in-plane (xy) CTE does indeed contribute more to the z strain than a out-of-plane (z) CTE of the same magnitude. With a Poisson's ratio of zero, the in-plane CTE does not contribute to the out-of-plane expansion. Hence, the Poisson's ratio and the in-plane CTE contribute significantly to the stress in the via.

#### **4.1.4.3 Examination of Trends**

There are essentially three things we can do to reduce the strain in the via wall. They are:

1. Make the via wall more compliant, so that it can accommodate more strain.

2. Drive less strain into the via wall.

3. Increase the strength (cross sectional area) of the via wall.

Each of the variables tested affects the strain results by one of these three methods.

Examining the summary of results in Table 4, we find that the four biggest factors affecting the strain are top drill width (tdrillw), via wall thickness (wallthk), the base material (basemat), and epoxy1 material (epox1mat).

Increasing the top drill width (tdrillw) makes the via wall longer by making the wall less steep. A longer wall accommodates more deflection with the same strain and thus is more compliant.

Increasing the via wall thickness (wallthk) increases the stiffness and the strength of the wall together. The net result is a reduction in stress and strain in the wall. However, the top pad thickness (tpadthk) should not be increased with the wall thickness. If this is done, the thicker top pad will attempt to constrain the Kapton layer more, thus forcing 6% more strain into the via wall.

Changing the base material from silicon to Kapton allows the dielectric and epoxy material to bulge under the via as well as over it, as explained before (see Figure 23), thus driving less strain into the via. Of course we cannot practically make chips out of Kapton, however this example does show the point.

Changing the Ultem on level zero to SPI EPOXY increases the via strain about 12%. The higher expansion coefficient of SPI EPOXY is responsible for the increased strain. While higher strain is not desirable, we can conclude that an epoxy with a lower thermal expansion would result in lower via strains.



Although we did not test any changes on the dielectric material (Kapton), we can conclude from the other tests that a lower thermal expansion material would result in lower strains, since it would better match the expansion of the via.

Changing the boundary conditions so that the total radial expansion matches that of alumina reduced the strain almost 8%. This reduction is due to the resulting smaller Poisson contribution to z strain. However, since the radial expansion essentially matches that of the attached chip, we cannot really effect this change without changing the chip material. This is obviously unlikely.

Of the other parameters tested, none had more than a 5% effect on the via strains.

#### **4.1.5 Two-Dimensional Local Model Discussion Summary**

- The linear two-dimensional axisymmetric model correctly predicts the locations of the strain concentrations.
- The linear model should not be used for absolute values of stress or strain.
- The linear model can show trends and can be utilized in comparison studies.
- The largest strain concentration, in both size and magnitude, occurs just below the dielectric/epoxy interface, on the inside of the via barrel in the corners. However, the location relative to the material interface is only a coincidence.
- No strain concentration exists at this location away from corners, as determined from the plane strain model.
- The entire via barrel section yields at 120 °C, and -65 °C.
- The via barrel strain can be reduced by:
  - Increasing the compliance in the via wall.
    - Make the via wall less steep. - verified
    - Make the via wall curved, instead of straight. - unverified

- Increasing the strength of the via wall.
  - Increase the via wall thickness. - verified
- Reducing the load (strain) placed upon the via.
  - Use more compliant material below the via. - verified
  - Use dielectric materials, and epoxy material materials that better match the via in coefficient of thermal expansion and Poisson's ratio. -verified

Unfortunately, the material properties of Si, Kapton, or the epoxies are not easily changed. Hence, at this point the only practical recommendations are to increase the via wall thickness and make the via wall less steep.

#### **4.2 Family of Three-Dimensional Finite Element Models**

This family of models offers the potential for the highest degree of accuracy. However, due to the nature of three-dimensional non-linear analyses, even a relatively course mesh consumes prohibitive amounts of computers resources. The three-dimensional analysis is used primarily to verify the results of the two-dimensional non-linear axisymmetric analysis.

With this in mind, the same assumptions, base model geometry and boundary conditions are utilized in both models. Also the two-dimensional model was remeshed to match the mesh of the three-dimensional model. This involved lowering the mesh density of the two-dimensional model and using non-mid side node elements. This should improve correlation between the two models by removing mesh discretization differences.

#### 4.2.1 Element Plots

Figure 24 shows the element plot for this model. Although the mesh outside the via is not shown, it should be noted that the mesh density there is quite low. This was done so that a reasonably fine mesh could be placed in the area of interest, the via. This approach should allow us to achieve good results in the via with a reasonable computational cost.

#### 4.2.2 Discussion

Examining Figures 25 and 26 we see that the results of two-dimensional and three-dimensional model match quite well both qualitatively and quantitatively. The three-dimensional model shows a large stress concentration on the lower inside via corner, just as expected from the two-dimensional results. Also the maximum stresses at that concentration match within 10%, with 0.012 for the two-dimensional model and 0.012 for the three-dimensional model. Hence, with the two-dimensional axisymmetric model, little is lost in terms of accuracy, while great benefits are gained in computational costs.

Also examining Figures 25 and 26 again we see that strain concentration is reduced at the mid plane of the via, as predicted by the two-dimensional plane strain/stress model. However the results at the mid plane do not match quantitatively. The three-dimensional model predicts yielding throughout the wall, where as the two-dimensional plane stress/strain model does not. Without yielding the two-dimensional plane stress/strain model grossly under predicts the strains.

It should be noted that in this case both models were cycled through only two hysteresis loops. The result is that the maximum stress does not occur at the primary stress concentration. However, analysis shows that the maximum stress will move to the primary stress concentration

at or around the 3<sup>rd</sup> hysteresis loop. This was not done at this time since we are only interested in comparing the models under equivalent conditions.

### 4.3 Chapter Summary

The following results were concluded from the family of two and three-dimensional models.

- The linear two-dimensional axisymmetric model correctly predicts the locations of the strain concentrations, so that it can be used for qualitative analyses.
- The non-linear axisymmetric model predicts the strain within 10% of the three-dimensional model.
- The largest strain concentration, in both size and magnitude, occurs just below the dielectric/epoxy interface, on the inside of the via barrel in the corners. Note that the location relative to the material interface is only a coincidence
- Away from the corners the stress concentration is reduced.
- The entire via barrel section yields at 120 °C, and -65 °C.
- The via barrel strain can be reduced by:
  - Increasing the compliance in the via wall.
  - Increasing the strength of the via wall.
  - Reducing the load (strain) placed upon the via.

Parameter (Model Name)	Parameter Description	Base Model Value	Changed Parameter <sup>1</sup> Model Value
Geometry Parameters (μm)			
epoxhgt1	height of epoxy 1	10	15
lpadthk	landing pad thickness	2	4
tdrillw	top drill width	45	60
tpadthk	top pad thickness	4	6
tpadw	top pad width	72	100
wallthk	via wall thickness	4	6
Material Parameters			
basemat	base material	Silicon	Kapton
epox1mat	epoxy 1 material	Ultem	SPIepoxy
lpadmat	landing pad material	Aluminum	Acid Copper
Other Parameters			
linear	type of stress - strain relationship	Yes	No
plstrain	determines two-dimensional modeling assumption	Axisym- metric	Plane Strain

<sup>1</sup> Note one model was created for each changed parameter listed, with the only difference from the base model being the changed parameter.

Table 3. Parameter key for the two-dimensional family of via models.

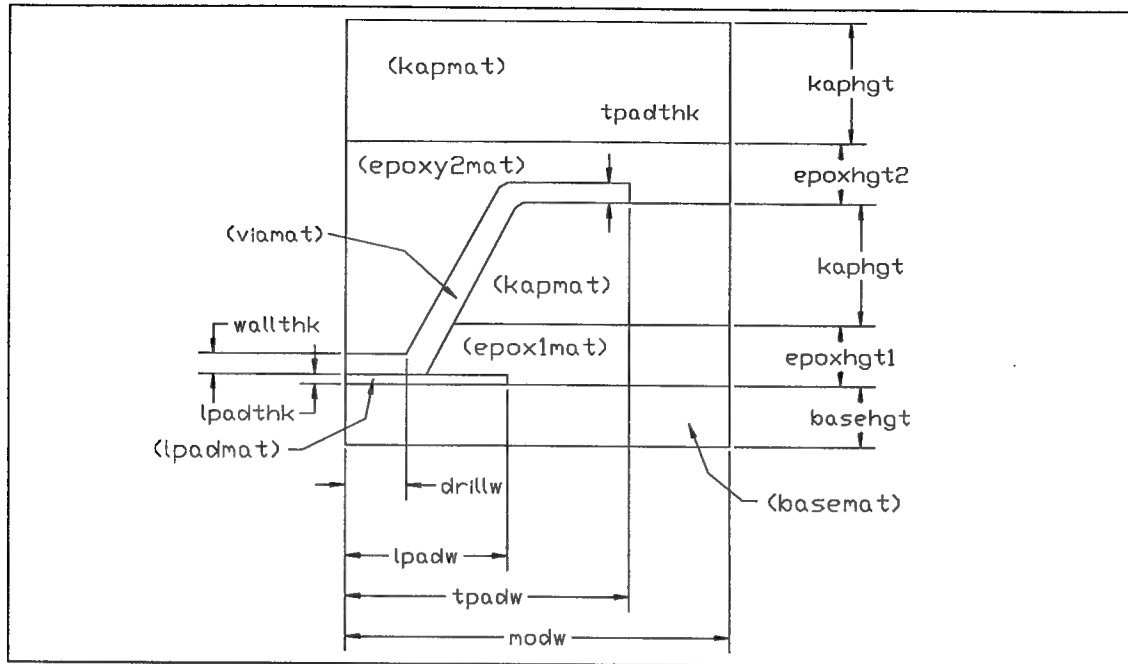


Figure 18. Geometry of axisymmetric via model family. Note that dimensions, as well as material are parameters and can change from model to model. Material parameters are shown in parentheses.

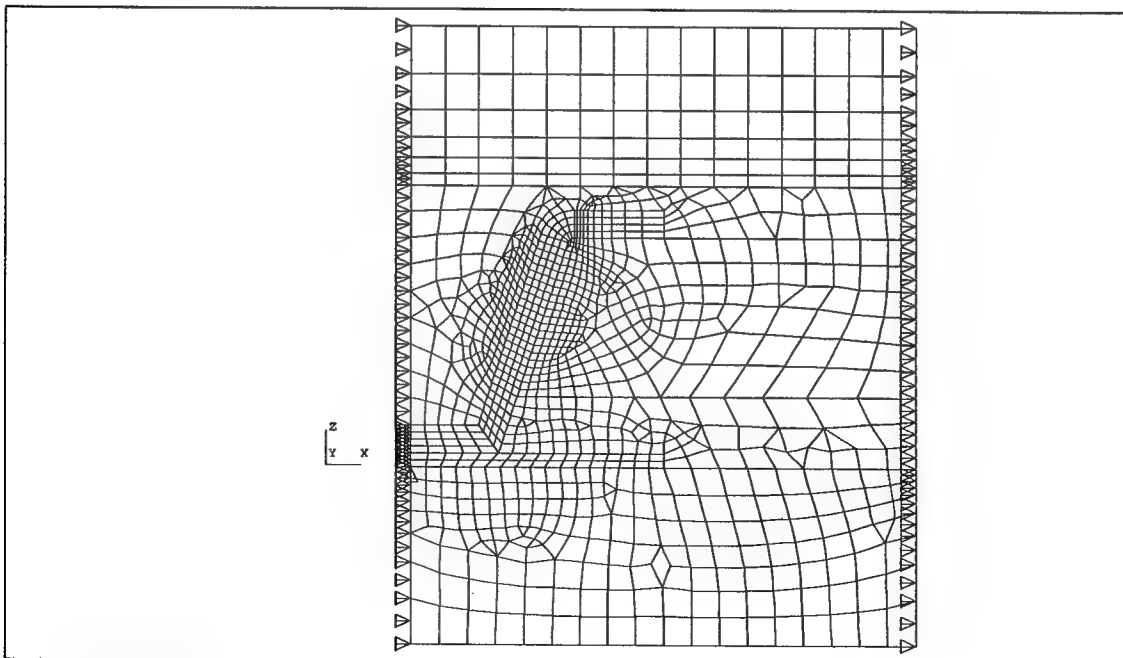


Figure 19. Boundary conditions and element plot for the base axisymmetric via finite element model. Note that the mesh of a specific model will depend upon geometry parameters.

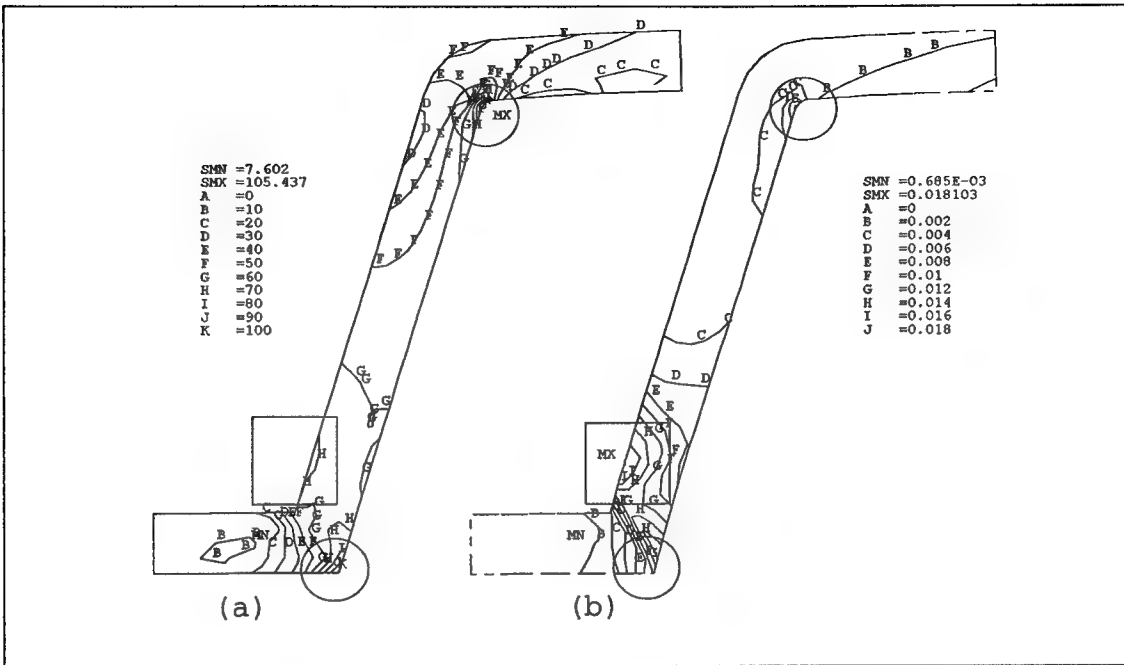


Figure 20. Effective structural strains in a via with the base geometry at 120 °C. (a) Normalized linear model. (b) Non-linear model. Note the von Mises criterion is used to determine effective strain. The second and third largest concentrations are circled on both plots, with the largest concentration being squared.

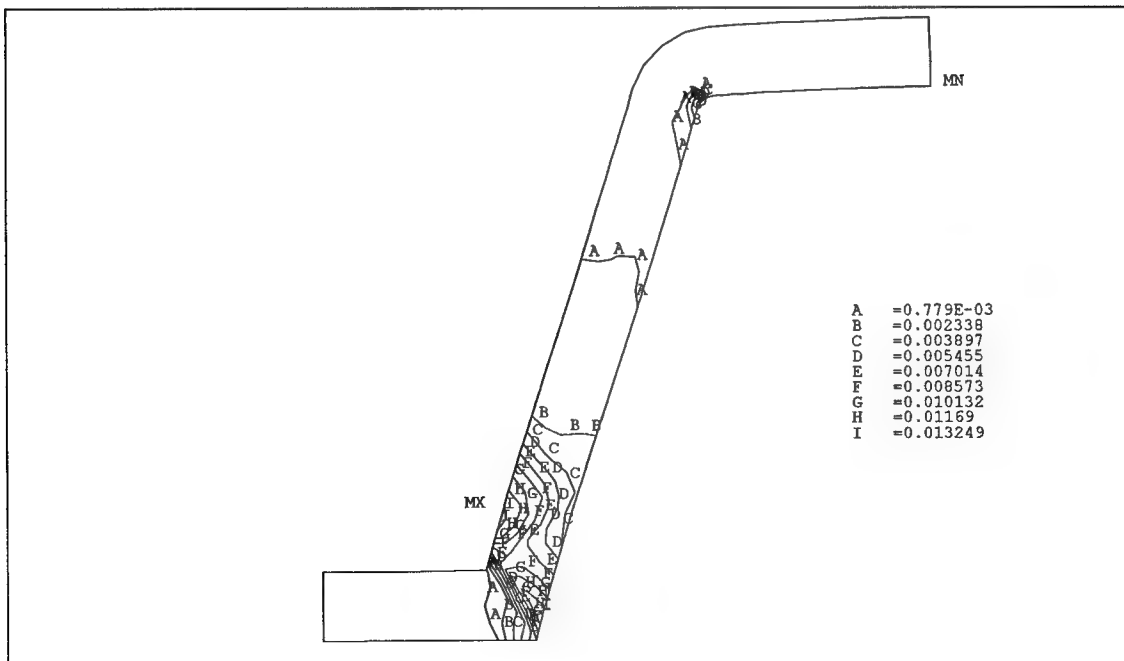


Figure 21. Plastic effective structural strains in a via with the base geometry at 120 °C.. Note that the entire via wall has yielded.

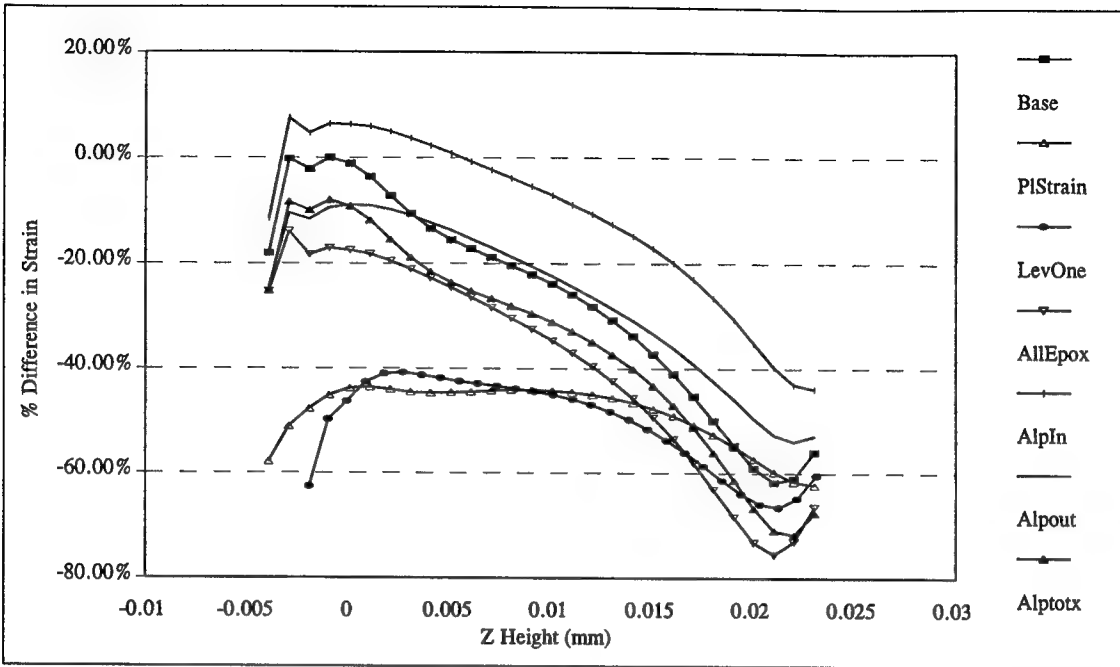


Figure 22. Effective structural strain vs. Z location along the inside via wall. The x axis zero represents the Kapton/Ultem interface. Linear model with temperature range from -65 °C to 120 °C.

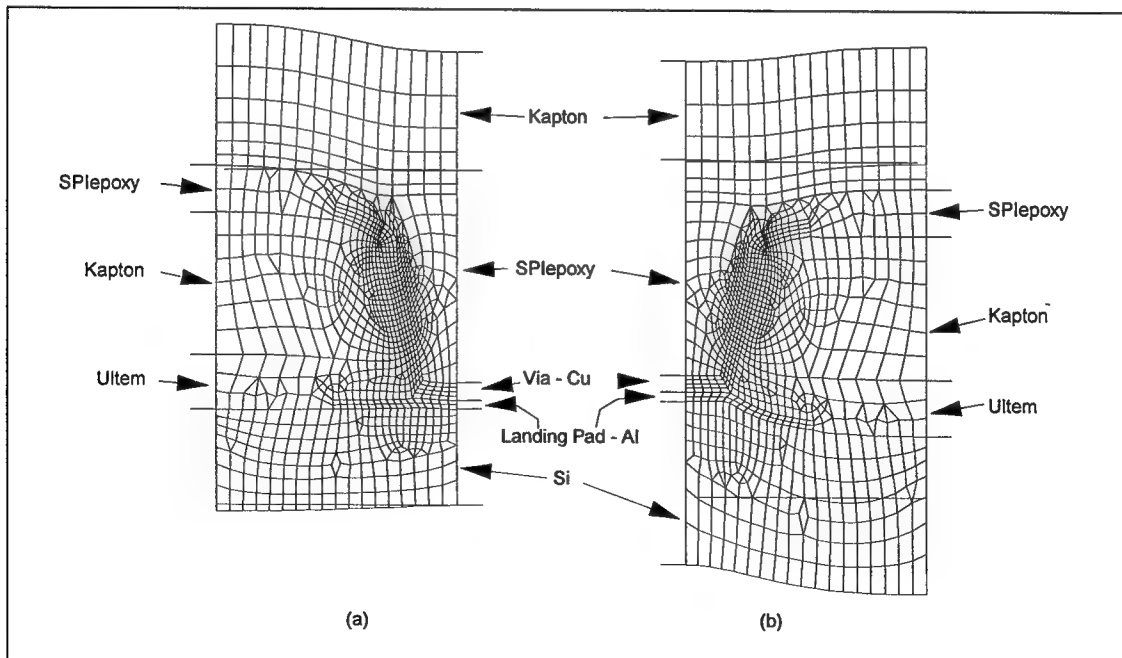


Figure 23. Displacement plots of (a) level zero and (b) level one via. Observe that the via wall has higher strain in the level zero via.



Variable Changed	Change	% Change of Stress		% Change of Strain	
		von Mises	1st Principal	von Mises	1st Principal
None (Base Model)	---	0.00%	0.00%	0.00%	0.00%
Geometric Variables ( $\mu\text{m}$ )					
epoxhgt1	10 $\Rightarrow$ 15	4.24%	-0.45%	4.29%	3.81%
lpadthk	2 $\Rightarrow$ 4	-1.29%	-0.05%	-1.35%	-1.09%
tdrillw	22.5 $\Rightarrow$ 30	-14.03%	-15.63%	-13.99%	-13.93%
tpadthk	4 $\Rightarrow$ 6	6.16%	6.34%	6.19%	6.18%
tpadw	36 $\Rightarrow$ 50	-1.14%	-0.97%	-1.17%	-1.03%
wallthk	4 $\Rightarrow$ 6	-12.36%	-9.00%	-12.43%	-11.01%
Material Variables					
basemat	Silicon $\Rightarrow$ Kapton	-53.71%	-55.34%	-53.83%	-55.38%
epox1mat	Ultem $\Rightarrow$ SPI EPOXY	8.65%	10.55%	8.51%	8.81%
lpadmat	Aluminum $\Rightarrow$ Copper	2.12%	2.22%	2.08%	2.30%
Other Models					
LevOne	Levzero $\Rightarrow$ Levone	-48.45%	-48.71%	-48.55%	-50.11%
Plstrain	Axisymmetry $\Rightarrow$ Plane Strain	-43.50%	-57.86%	-43.56%	-48.54%
AllEpox	SPI EPOXY & Ultem $\Rightarrow$ SPI EPOXY	-13.60%	-13.95%	-13.90%	-14.21%
AlpIn	Pseudo Mat. 1 <sup>1</sup>	7.28%	-9.74%	7.52%	1.82%
AlpOut	Pseudo Mat. 2 <sup>2</sup>	-9.14%	-10.46%	-8.94%	-9.15%
Alptotx	Radial Disp = 0 <sup>3</sup> $\Rightarrow$ CTE <sub>alumina</sub> * $\Delta T$ * (model rad)	-7.96%	-7.72%	-7.98%	-8.18%

<sup>1</sup> Stiffness is 1/10th that of copper. In-plane and out-of-plane CTE is 5\*CTE<sub>copper</sub> and CTE<sub>coppers</sub> respectively.

<sup>2</sup> Stiffness is 1/10th that of copper. In-plane and out-of-plane CTE is CTE<sub>copper</sub> and 5\*CTE<sub>coppers</sub> respectively.

<sup>3</sup> Models the effect of the via attached to alumina, rather than attached to silicon.

Table 4. Stresses and Strains of two-dimensional family of via models at 120 °C. Results normalized to the maximum equivalent strain in the base model.

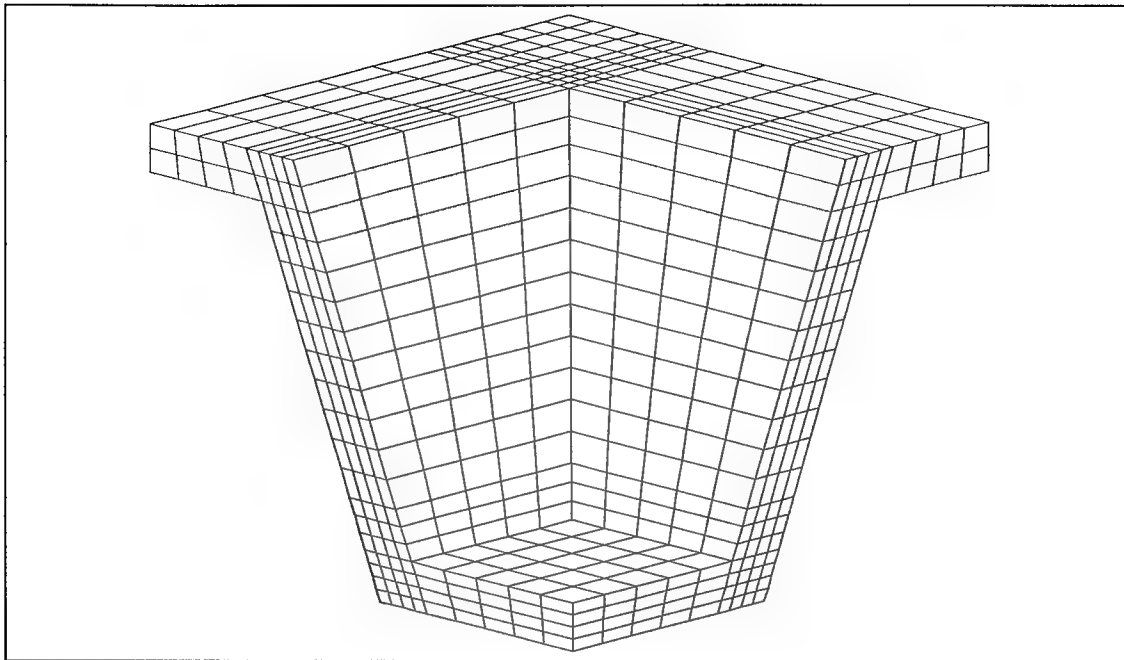


Figure 24. Three-dimensional local via model element plot. Note that only the actual via is plotted.

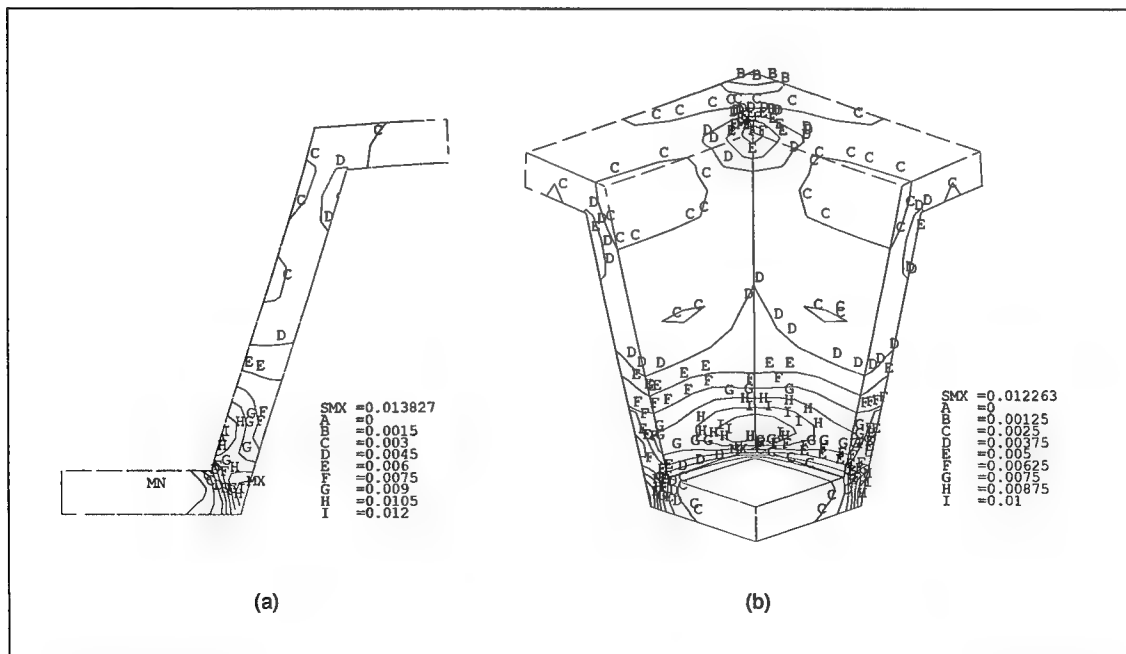


Figure 25. Elastic + Plastic von Mises strain in (a) the axisymmetric model, and (b) the three-dimensional model. Note that this model was cycled through only two hysteresis loops, resulting in relatively low stresses.

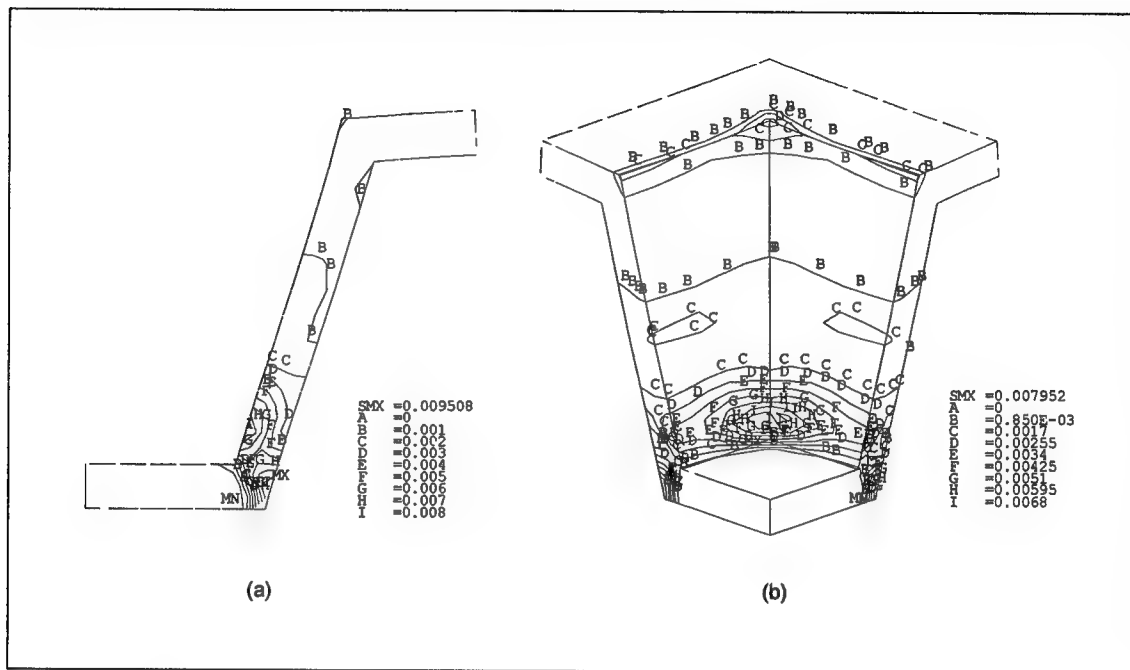


Figure 26. Plastic von Mises strain in (a) the axisymmetric model, and (b) the three-dimensional model. Note that this model was cycled through only two hysteresis loops, resulting in relatively low stresses.

## CHAPTER 5

### EMPIRICAL CALIBRATION

Using finite element analysis one can generally obtain a wide variety of results depending upon the input parameters. Indeed, it is difficult to determine if the results bear any resemblance to reality unless one can calibrate the model with empirical data. Fortunately we were able to obtain empirical calibration data with the assistance of David Read and Elizabeth Drexler of the Nation Institute of Standards and Technology (NIST) Boulder Laboratories, Boulder, CO.

In this chapter we will briefly review the technique used by Read and Drexler and compare the NIST empirical data to the finite element data. For a more detailed explanation of the empirical technique, see Read *et. al.* [10]

#### 5.1 Empirical Technique

Electron-beam moiré was the technique used to determine the total z strain in a via. Simply described, electron-beam moiré determines the displacement of a point by examining an interference pattern between a stressed and a non-stressed specimen. The interference pattern is created by carefully grating the specimen and showering the grating specimen with electron beams.

With electron-beam moiré, high magnification and resolution is possible. However, it also has difficulties and limitations. Some of the difficulties are listed below:

- Electron-beam lithography, a difficult process, is required to produce the precise high density gratings and cross gratings required.
- It is not yet possible to measure the displacements in both x and y directions from the same field.
- The specimen must be placed within a vacuum chamber for the scanning electron microscope (SEM).
- The specimen must be sectioned so that a cross section of the via is exposed. This not only presents the potential of damage to the specimen, it also disturbs the fundamental state of stress of the part.
- Strains are not directly observed. Rather, they are computed by numerical differentiation of the observed displacements. Recall that differentiation tends to exaggerate errors.

However in this situation the limitations are either not an issue or can be overcome by careful attention to detail.

#### **5.1.1 Sample Preparation**

The first step in the specimen preparation was to produce a very flat cross-section through the via. Since the z strains (through the thickness) are of primary interest, the cross section exposed the XZ plane. The section was then potted in epoxy and prepared using metallographic - style procedures. The sample was then sanded with a very fine grit paper, and the final polish was obtained with a natural diamond aerosol spray, so that a smooth surface through a via was exposed. The sample was then swabbed with methanol and cleaned in an ultrasonic methanol bath. Finally the surface was scrubbed with acetone on a soft polishing cloth. Within two hours of the final polish and cleaning, the specimen was sputter-coated with AuPd.

The gratings were applied using electron-beam lithography. 512 lines were applied with a pitch of 175 nm. The lines were created perpendicular to the z direction to enable measurements of z direction deformation.

### 5.1.2 Recording of the Moiré Fringe Patterns

To observe thermally-induced displacements, the specimen was mounted on a heating stage pad within the SEM. Careful attention was paid to ground the heater and stage to avoid distortion of the SEM image. Two thermocouples were then attached; one to the heater, and an other between the specimen clamp and specimen. Then the magnification of the SEM was adjusted to create the moiré fringe. Note that three fringes are present at room temperature rather than a null field (an exact match between the line pitch and the pitch of the rastered electron beam) due the discrete magnification settings of the SEM. The specimens were then brought to temperature, and the resulting increase in fringes were observed. See Figure 27 for examples of the observed fringes. Note that the samples were held at temperature for approximately 30 min. to ensure that thermal equilibrium was reached.

## 5.2 Data Reduction

Data reduction was begun by manually tracing the fringes to produce a list of x, z pairs giving the location of each fringe. Spline fitting was used to interpolate fringe numbers from the traced points to a regular grid. The z displacement, w, was taken at each of these points at each temperature. The strains were then found by using  $\epsilon_{zz} \approx \Delta w / \Delta z$ . This data was then interpolated from about 10 actual fringes, at the highest strains, to a total of 25 z positions. Data was also taken at 25 x positions to yield a grand total of 625 data points for each temperature observed.

### 5.3 Modeling Technique

The two-dimensional via model used in **Chapter 5** was chosen to calibrate with the NIST data because it gives us the speed needed to modify and rerun the analysis to improve calibration. However, two modifications were required of the model before calibration could begin. First the geometry of the via was changed to match the tested via as closely as possible (the geometry information was retrieved by measuring a photograph of the actual via tested). Second, we used a plane stress model.

We chose a plane stress model to mimic the effect of the free surface exposed by the experimental technique. Note that the exposed surface should result in stresses significantly lower than in the native via environment. However, if we can calibrate the via stresses in this environment, we are more likely to have accurate stresses in the native environment.

### 5.4 Discussion

#### 5.4.1 The Finite Model Results

Before we compare the model results and the electron beam moiré (EBM) data we should take time to review the model results outside of the via, since the experimental resolution has some difficulty in detecting via strains.

In Figure 28 we show the effective total coefficient of thermal expansion in the z directions ( $\alpha_{z\_tot}$ ) rather than the total strain. This allows us to compare the actual expansion to free expansion, to achieve a better understanding of the state of stress in the via. Remember that  $\alpha_{tot}$  is simply the total strain (mechanical and thermal) divided by the change in temperature ( $\epsilon_{tot}/\Delta T$ ).

We see that much of the model away from the via is simply expanding freely. The Si below the via, the Kapton above the via, and the epoxy and Kapton radially away from the via are all expanding close to their respective free expansion rates (see Appendix B for material properties). Indeed given the assumptions of the model, this is what we should expect. The only areas where the expansion is markedly different than free expansion is in the via itself, in the epoxy inside the via, and in the epoxy directly above the via.

The via wall is in tension. Given that the CTE of copper is roughly one fifth that of Kapton, this result is not surprising. The epoxy inside the via wall is in compression. This is due to the lack of expansion of the via, which then constrains the epoxy.

The epoxy above the via walls have the highest tensile strains in the model. This is due to the relatively low stiffness of the epoxy and low thermal expansion of the copper. Since the copper expands relatively little, it pulls down upon the epoxy. Since the epoxy has low stiffness relative to the copper and Kapton, its strains are relatively high. If the epoxy were stiffer then more strain would be driven into the Kapton above the via, and less into the epoxy. If the epoxy layer was thicker, then there would be more material to absorb the lack of expansion of the copper, and the epoxy strain would be lower.

While the strains outside the via are high, recall that strains in the via are of primary concern. Although the strains in the rest of the model are much higher, the stiffness is much less, so that it behaves not unlike a rubber band. Hence, the strains in the rest of the model are really only relevant as far as experimental calibration is concerned. Remember that lack of resolution prevents experimental calibration with the via strains.



### 5.4.2 Data Comparison

In order to better compare the data, the data will be presented in XY graphs where  $\epsilon_z$  is along the Y axis, and "distance along a path" on the X axis. The paths are shown on Figure 29.

Figures 30 - 35 compare the EBM data and the finite element analysis along several given lines. Upon examining these graphs we find that calibration is quite good in the layer of the via, but it is very poor outside of that layer. For example, both the analysis and the data find that the expansion of Kapton is about 0.0115 at 120 °C (Figure 33) corresponding to the free expansion of Kapton. However, above the via the EBM data shows the Kapton in tension (Figure 35 shows an expansion of  $\sim 0.016$ ) while the analysis still shows free expansion. Indeed, it is difficult to determine a plausible reason why the Kapton above the via would be in tension.

Also, below the via we find the same trend, the NIST data showing considerably higher strains than the analysis. However, upon examining the sample, NIST personnel found a crack in the Si (below the via), and partial delimitation between the epoxy and Kapton (above the via). This delamination shows up as a step increase in displacement, which would then increase the strain and thus account for the discrepancy between the NIST data and the analysis. Since the defects in the sample occurred despite very careful handling, the fragility of the via cannot be understated.

Figure 32 (path h) highlights a flaw with the experimental technique. The finite element data shows a severe dip in expansion around 50  $\mu\text{m}$ . Since the path passes through Cu in this area, the strains MUST drop. However, the experimental technique does not show this. This is due to the

migration of the fringes in the interference pattern toward the areas of high strain. While this migration improves resolution in areas of high strain, it reduces resolution in areas of low strains.

Figure 33 (path J) shows the best calibration. This path passes horizontally through the center of the via, and shows reasonable calibration in all three regions: the epoxy, the via, and the Kapton. Since we get reasonable calibration in the area of concern, we can conclude that the finite element results are reasonably accurate.

## 5.5 Chapter Summary

Difficulties with the experimental technique, and lack of confidence in the material properties make calibration of the model with the NIST data a formidable task. However, we were able to show reasonable calibration in the layer of via, as shown by a strain of 0.0115 in the Kapton by both the analysis, and the experiment.

Out of the layer of the via we find poor agreement. This lack of correlation can be explained by cracking and delamination in these layers that occurred during sample preparation despite careful measures to prevent such damage.

An other area of large disagreement was in the top landing pad. The analysis showed strains reasonable for copper, while the NIST data showed strains reasonable for a polyimide (like Kapton). Since the top landing pad is thin, and the via is made of copper, we conclude that the experimental technique is unable to detect localized dips in strain.

The disagreement in the data highlights two difficulties with the experimental technique. First, the samples are damaged easily, so that extreme care in preparation is required. This is seen

in the aforementioned results of delamination. Second, the technique cannot detect localized dips in strain, as seen in the aforementioned strains in the top landing pad.

The general results of the model make sense intuitively, and we have quantitative calibration in an area of the sample that we believe is undamaged. Hence, we conclude that the non-linear model provides a reasonable qualitative and quantitative representation of the stress/strain field in the via.

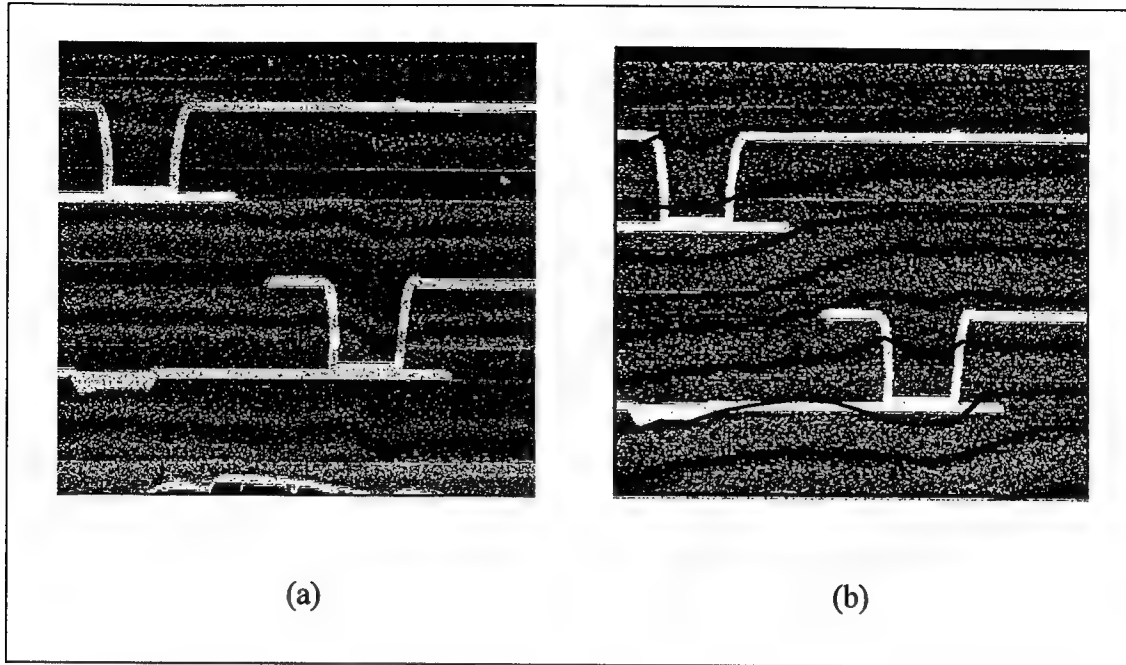


Figure 27. The moiré fringe pattern at (a) 24 °C, and (b) 151 °C. Note that the fringes are traced in (b) so that they are easily visible.

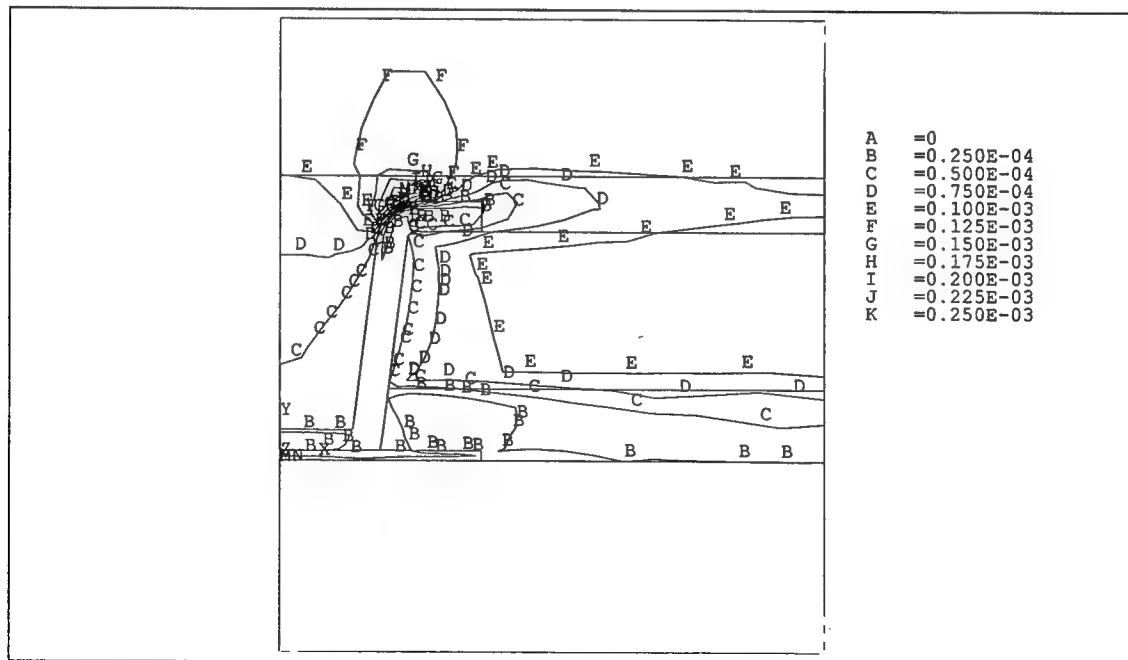


Figure 28. Normalized finite element z strains (i.e... total z expansion rate,  $\alpha_{z\_tot}$ ) for a plane stress model with NIST geometry.

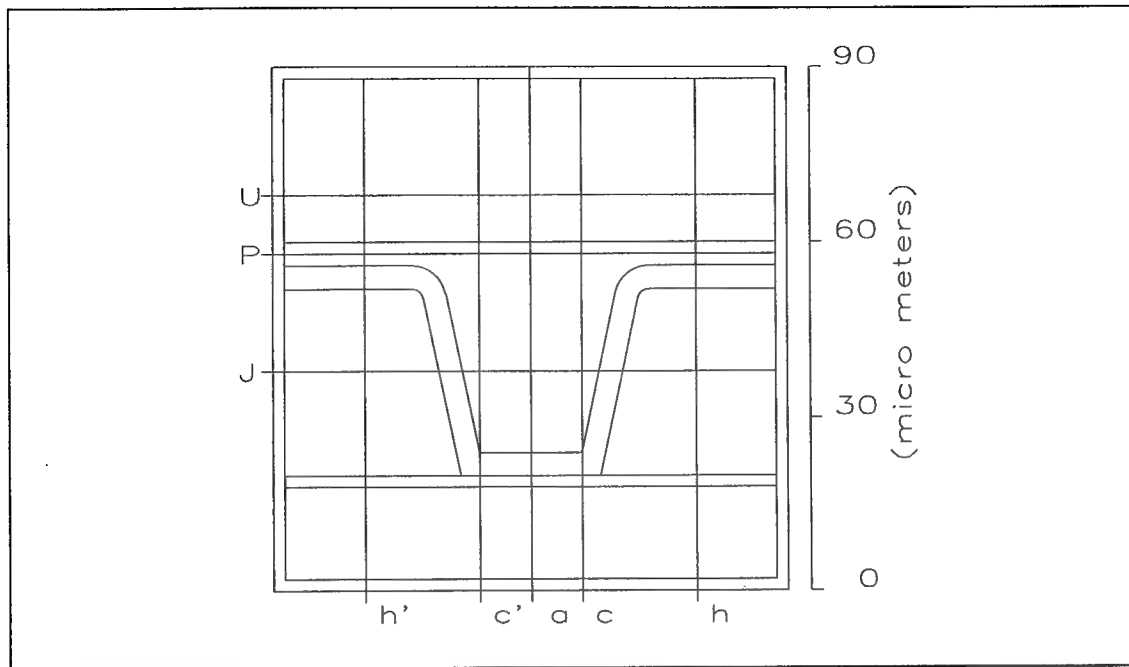


Figure 29. Data acquisition paths for empirical/analytical data comparisons. The uppercase and lowercase letters represent horizontal and vertical paths respectively. A (') represents a path symmetrical about the via center plane.

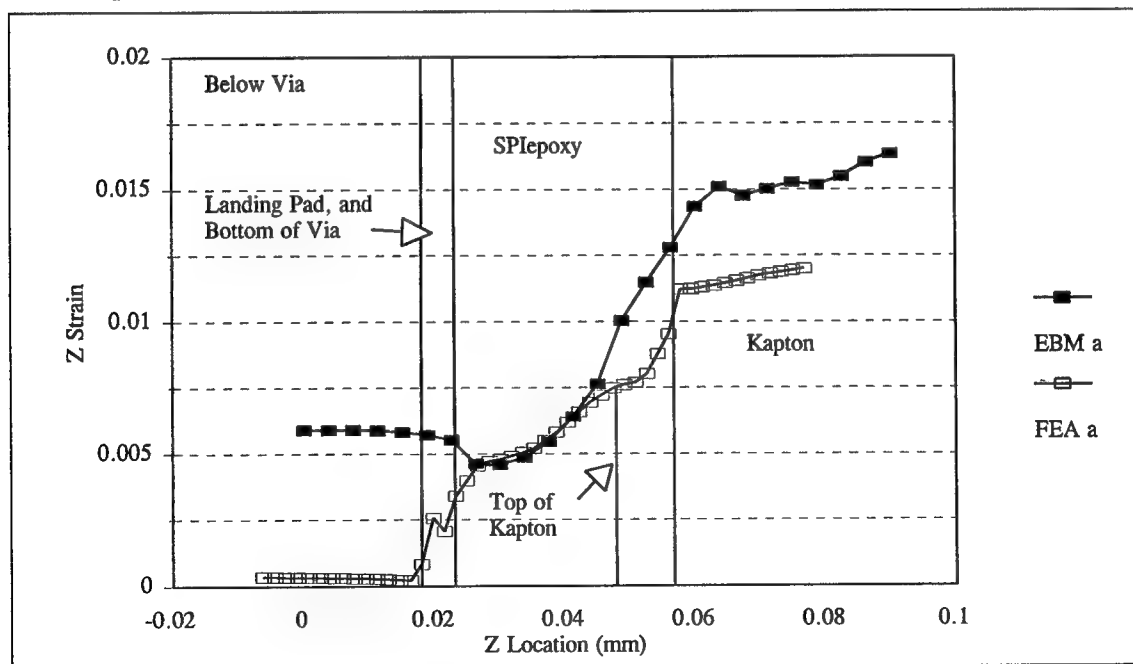


Figure 30. EBM data vs. finite element analysis for path a/a' (Center of Via). Note that calibration is reasonable only in the layer of the via (first part of the SPI EPOXY layer).

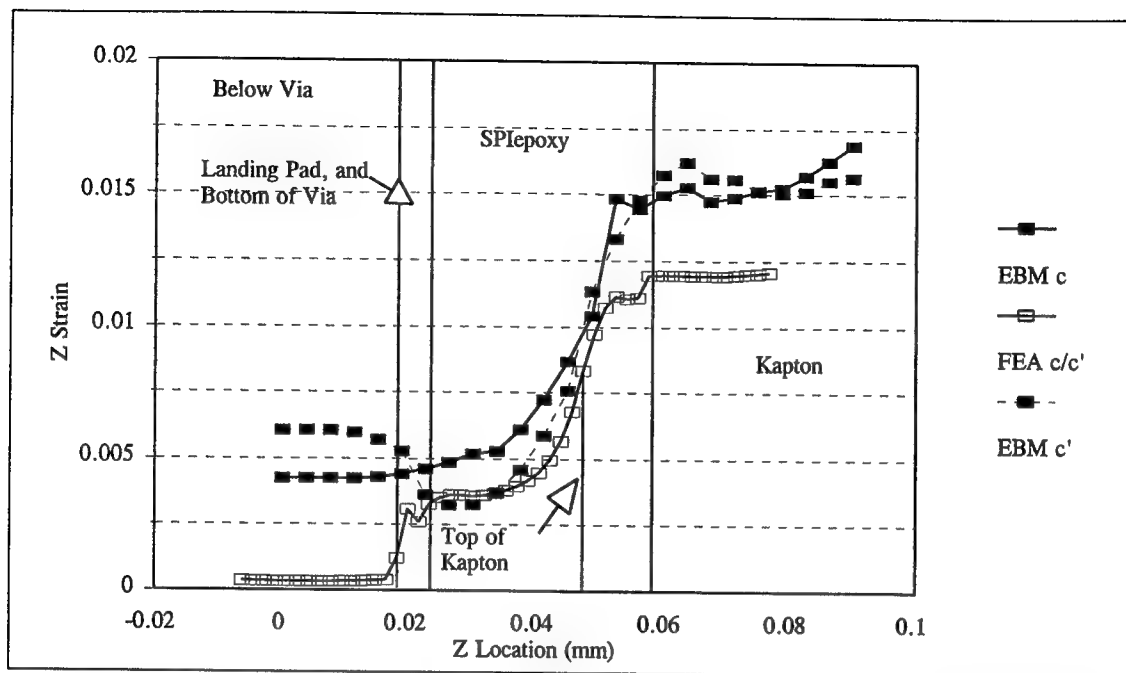


Figure 31. EBM data vs. finite element analysis for path c/c' (Near Via Inside Wall). Note that calibration is reasonable only in the layer of the via (the first part of the SPI EPOXY layer).

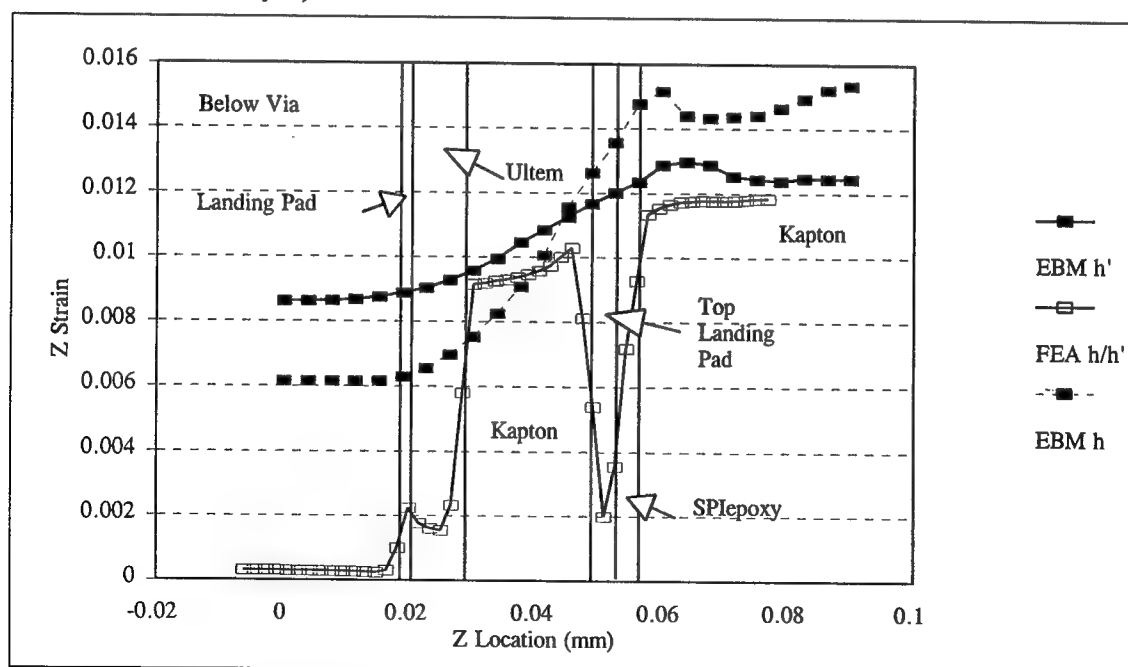


Figure 32. EBM data vs. finite element analysis for path h/h' (Outside of the Via). Note that calibration is reasonable only in the layer of the via (Kapton only).

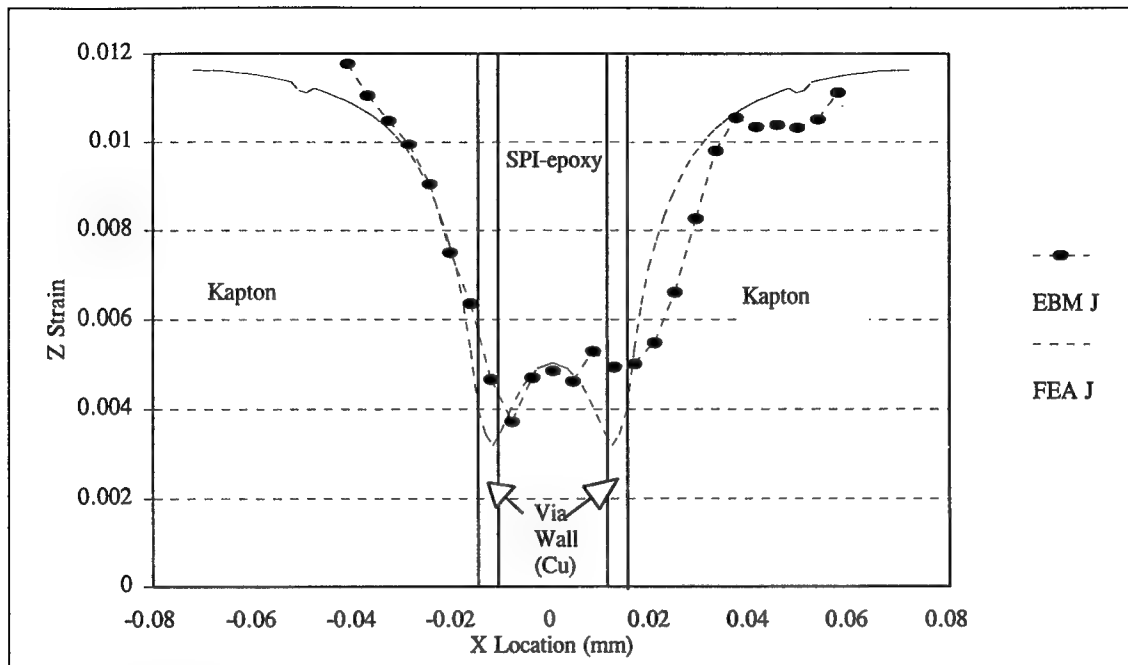


Figure 33. EBM data vs. finite element analysis for path J (Through the Via Layer). This path shows the best calibration.

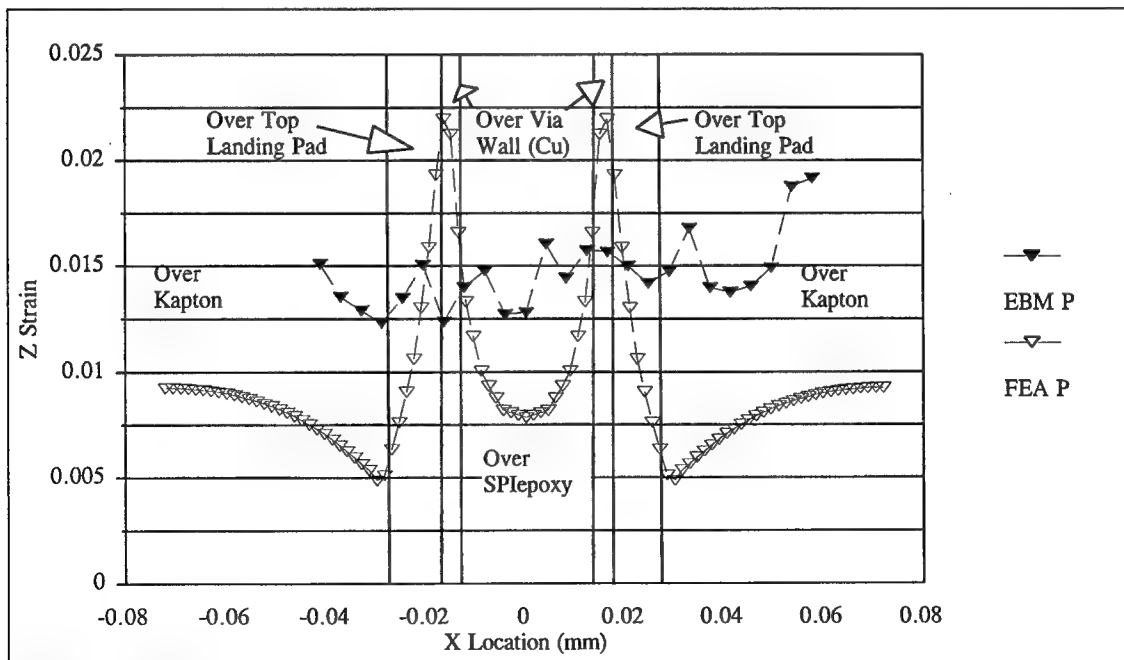


Figure 34. EBM data vs. finite element analysis for path P (Through the Epoxy Layer). This layer should be all epoxy.

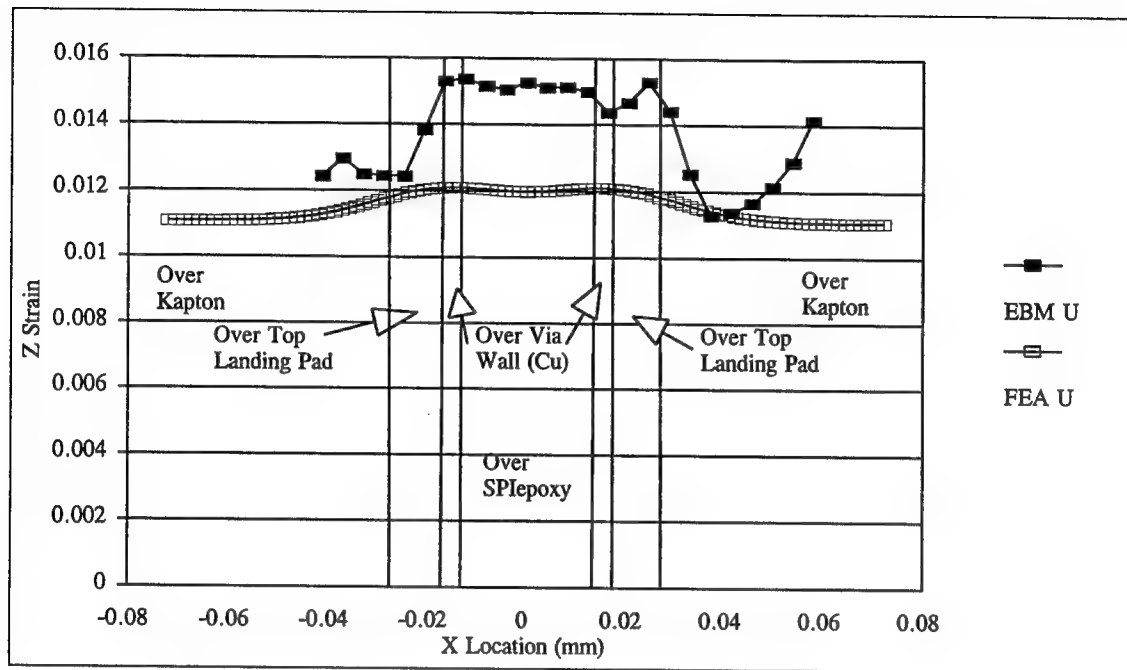


Figure 35. EBM data vs. finite element analysis for path U (Through the Top Kapton Layer). This layer should be all Kapton.



## CHAPTER 6

### MODELING GUIDELINES

This chapter contains information that may be useful for future modelers of vias or MCMs in general.

#### 6.1 Global Models

Global models typically are not required to determine the strain field in the interconnect layer. The strains in the interconnect layer are dominated by the chip and substrate, because of their relatively high thickness and stiffness. In fact, the total strain in the interconnect layer can be bounded by zero and the free expansion of the substrate. These limiting bounds produced less than 10% difference in the mechanical strains in the via model studied in this report. If more accuracy is needed, tighter bounding strains can be obtained with the analytical model discussed in **Chapter 3**. Considering the other uncertainties inherent in any model, the cost and effort of constructing a global model seems unjustified for most applications.

This should apply in any module where there is a high ratio of the product of the stiffness times thickness of the substrate-chip layer to that of the interconnect layer. In the case of the MCM studied in this report that ratio was almost 1200. However we suspect that this rule applies even with ratios as low as 100 or even 10.

Even in transient models or models with non-uniform temperature loading, a global model should not be required. The microscopic dimensions of the local model keep the actual gradient across the local model from becoming significant. Reference [4] provides more information on transient models.

The one exception to this rule involves local models near chip or MCM boundaries. At free boundaries there is considerably less constraint upon the HDI layer, so that total expansion can be significantly greater than the free expansion of the substrate. At other boundaries significant shear can be introduced into the interconnect layer. Hence the effects of boundaries may require a global model to obtain boundary conditions for local models within close proximity of boundaries.

## **6.2 Isotropic vs. Orthotropic Material Properties**

Typically the interconnects layers are thin layers of polyimides and are inherently orthotropic. Work by Prahbu *et al* [4] indicates that orthotropic expansion coefficients will increase the stress in local models by about 10% over isotropic models. Hence, orthotropic material properties are preferred when available, but are not necessarily required to obtain good results.

It should be noted that no data was available for the effects of orthotropic Young's Modulus, Poisson's Ratio, or other mechanical material properties, so that their orthotropic effects are not known.

## **6.3 Plane Strain, Plane Stress or Axisymmetry**

When modeling a box-like structures such as an high density interconnect via, two-dimensional planar models are inappropriate. Planar models cannot account for the effects of the

side walls that lie off of the plane being studied. The side walls of the via significantly alter the magnitude and the distribution of the strain field.

The best two-dimensional modeling assumption for representing the true three-dimensional via structure is axisymmetry. In the case of the via studied in this report, the axisymmetric model matched the three-dimensional model within 10% at the corners of the vias.

#### **6.4 Linear vs. Non-Linear Analyses**

Our results indicate that linear models are appropriate for both global analyses and for *qualitative* local analyses. Linear models are not well suited to *quantitative* local analyses due to the high strains generated by the via. However, the linear models will correctly predict the locations, if not the magnitudes of the high strains, so that they can be used for comparing various model geometries. For more information on this, see **Chapter 4**.

#### **6.5 Via Stress Variation with Location**

The results showed that the via strain decreases with increasing via level (i.e. increasing distance from chip and substrate). However, past level zero the effect is largely negligible. The highest strain occurs within the level zero via (the via attached directly to the chip). The high strain in level zero is due to the high stiffness of the chip, which prevents the expansion of the dielectric below the chip, driving more strain into the via wall. More information on this can be found in **Chapter 4**. Thus, we recommend that analysis of vias in the chips-first technology begin with level zero.

## 6.6 Model Verification and Calibration

As in all analytical work, efforts should be made to verify and/or calibrate the results. The case of microelectronics presents several challenges to this goal, so that no hard and fast rules apply. In microelectronics the important model geometries often varies in dimension by orders of magnitude, making full three-dimensional models impractical. This forces one to use simpler models with built in assumptions that may not be appropriate. However, if several simple models can be built, each with different implicit assumptions, then confidence can be gained by the agreement of the different models.

The models need not be limited to finite element analysis. Analytical models can often be useful in verifying portions of a model. For instance in the case of this report an analytical model based upon beam theory correlated well with a shell model of the entire MCM and plane strain model of a slice of a MCM.

It is often difficult, if not impossible to obtain empirical in-situ data for calibration. However it is sometimes possible to obtain data for similar situations, and compare appropriate model results. For example in this report data for a sectioned via was obtained and compared with a plane stress model. While a plane stress model is inappropriate for a in-situ via, it is appropriate for a sectioned via, and it gives confidence in the in-situ model results.

By following these guidelines, the modeler should be able to construct accurate and robust models of vias, or other micro-electronic components attached to stiff substrates. Using these models we can determine the robustness of the designs and determine methods of increasing the quality and yield of the components.

## **CHAPTER 7**

### **CONCLUSIONS**

In the beginning of this report we sought to understand the modes of failure of vias in Multi-Chip Modules. To accomplish this objective we developed both global and local two and three-dimensional FEMs of high density MCM packages and via interconnect structures. Local models were validated by comparison with electron beam moiré data taken by NIST for the case of a sectioned via.

Our research on the global MCM structure indicates that the total strain in the HDI layer is dominated by the chip and substrate, due to their high stiffness compared to the HDI materials. Hence, the material properties of the HDI layer are not required to determine the global strain field in that layer. Also the global strains throughout the MCM are low enough so that there is no plastic deformation. Hence linear elastic global models are appropriate for thermomechanical models of MCMs under uniform temperature loading.

Two global analytical models were created to estimate the bounding strains in the HDI layer. The first model was based upon beam theory, and it over predicts the upper bound strains by about 10% and predicts the lower bound within 1% compared to the two-dimensional plane strain finite element models of xz planar slice of a MCM. The second model is based on the

simple assumption that the total strain lies between zero and the expansion of the alumina substrate. This proved to over predict the upper bound by at least 15% and predicts the lower bound within 1% compared to the two-dimensional plane strain finite element model.

Using the simple assumptions to produce upper and lower bound via wall strains produced only a 10% difference in strain. Since the impact of the bounding strain field is so small, it is not necessary to create sophisticated global models to obtain boundary conditions for detailed local via models; the simple assumptions are adequate.

Our local model research indicated that non-linear axisymmetry provides the best two-dimensional approximation for the three-dimensional local via model. The axisymmetric non-linear local model correctly predicts the location and magnitude of the strain concentration when compared to a three-dimensional local model.

The highest strain concentration is located at the lower inside corner of the via wall, so that this should be the most likely location for crack initiation. However, the axisymmetric and the three-dimensional model show that the entire via wall yields in tension at 120 °C and in compression at -65 °C, so that crack initiation at other locations should not be ruled out.

The linear axisymmetric model correctly predicts the location of the strain concentration. However it cannot model the yielding so that it is not quantitatively correct. The linear axisymmetric model was still found to be a valuable tool in qualitative analyses and in comparing various models.

A two-dimensional plane stress and plane strain model under predicts the elastic strains by about 40%. The plane stress and plane strain model incorrectly models the via wall as a sheet,

which is very compliant in bending. The actual via is stiffened at the corners by the side walls, thus causing higher strains in the corners.

The most significant factors that impact the via wall strain are:

- a thick via wall - a 50% increase in thickness decreased strain by 12%
- a non-steep via wall - decreasing the slope of the via wall from 72° to 60° decreased the strain 14%
- a thin top landing pad - a 50% increase in thickness led to a 6% increase in strain.
- softer material above and below the via - changing the base material from silicon to Kapton decreased the strain 54% (although a Kapton chip is not practical, it does show the point).

Although most of the via wall strain is in the out of plane direction, it was determined that the in-plane expansion coefficient of the HDI materials have a significant effect through Poisson expansion.

Previous investigators theorized that the dielectric/epoxy intermaterial boundary caused a significant strain concentration. However, no evidence of this phenomenon was found.

Comparison of the two-dimensional plane stress model results with the electron beam moiré data of a sectioned via showed agreement within 10%. A plane stress model is appropriate in this case because the sectioning of the via exposes a free surface, thus disturbing the in-situ state of the via. Currently there is no known method for collecting in-situ strain data for direct comparison with in-situ models.

Outside of the layer of the via agreement fell to 30-50%. This difference was attributed to damage of the specimen during sectioning. This damage highlights the difficulty of obtaining empirical data, since the specimen was handled with the utmost care.

## APPENDIX A

### FINITE ELEMENT MODEL INFORMATION

Analysis Program	ANSYS 5.0a
Chip Material	Si
Substrate Material <sup>1</sup>	Alumina (Al <sub>2</sub> O <sub>3</sub> )
Die Attach Material	SDAN
HDI Attach Material	Ultem
HDI Material Dielectric Material Epoxy Material	Kapton SPI EPOXY
Via Material <sup>2</sup>	
Via Landing Pad Material Level 0 Level 1	Aluminum Copper

<sup>1</sup> The local models did not model the substrate or die attach.

<sup>2</sup> The global models did not model the via, or via landing pad.

Table 5. Common model information for all the finite element models in this report.

Model Name	Element Type	Description	Element Options	Non-Linear
2D Global Plane Stress	Plane 42	4 node plane	Plane Stress	Yes
2D Global Shell	Shell 91	8 node shell 16 layers		No
2D Local Axisymmetric	Plane 82	8 node plane	Axisymmetric	Yes/No <sup>1</sup>
3D Local	Solid 45	8 node brick		Yes

<sup>1</sup> In this family of models both linear and non-linear models were used.

Table 6. Unique model information for the finite element models in this report.



## APPENDIX B

### MATERIAL PROPERTIES

Material	Young's Modulus (GPA)	Poisson's Ratio	Coefficient of Thermal Expansion( $10^{-6}/^{\circ}\text{C}$ )	
			In-Plane	Out-of-Plane
Alumina	275	0.35	7	7
Aluminum	62	0.24	23.6	23.6
Silicon	190	0.28	2.5	2.5
Copper		0.34	17.6	17.6
at -65 °C	46.5			
at 20 °C	45.6			
at 125 °C	44.7			
at 200 °C	39.7			
at 300 °C	31.7			
Kapton™		0.35	20	112
at -65 °C	5.2			
at 23 °C	4.0			
at 100 °C	3.0			
at 350 °C	1.5			
Ultem™		0.35	56	29
at -65 °C	2.9			
at 23 °C	2.9			
at 100 °C	2.1			
at 350 °C	2.0			
SPI EPOXY		0.35	40	85
at -65 °C	3.3			
at 23 °C	2.5			
at 100 °C	1.5			
at 120 °C	0.9			
SDAN		0.25	10	35
at 23 °C	3.8			
at 100 °C	2.2			
at 350 °C	2.0			

Table 7. Material property data used throughout this report.

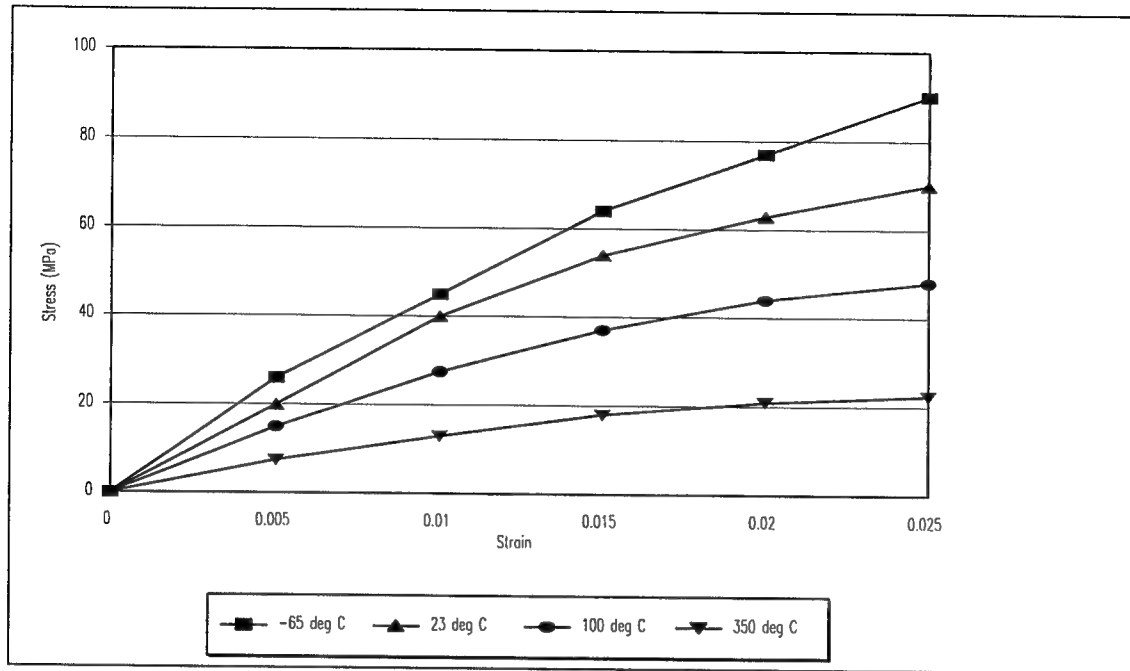


Figure 36. True Stress vs. True Strain curves for Kapton. [4]

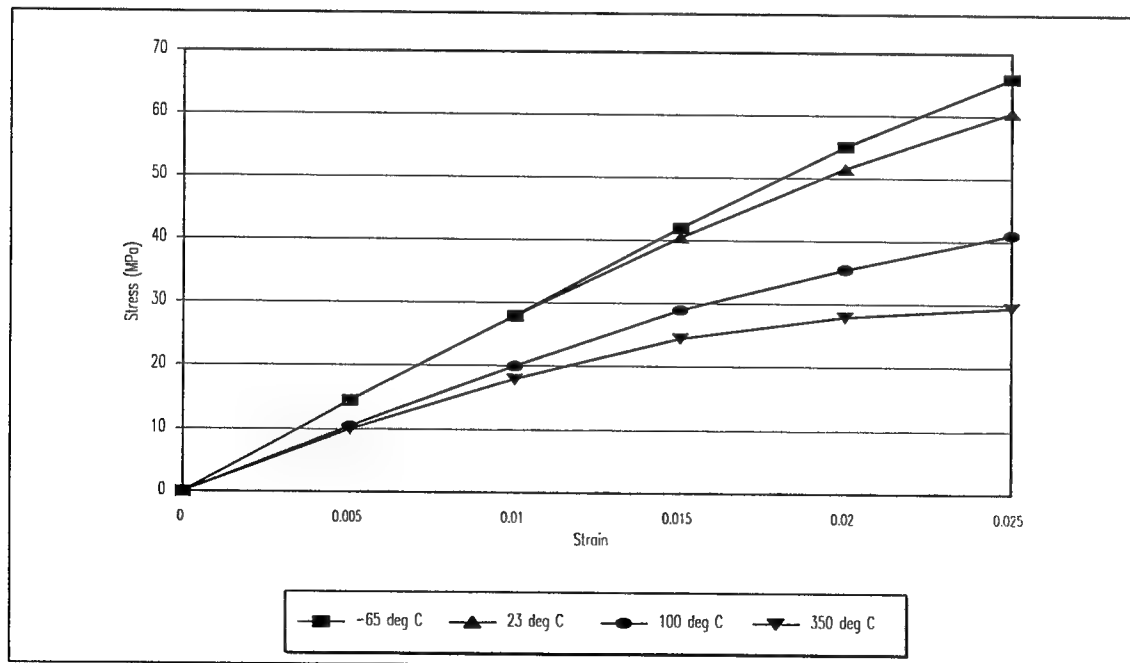


Figure 37. True Stress vs. True Strain curves for Ultem. [4]

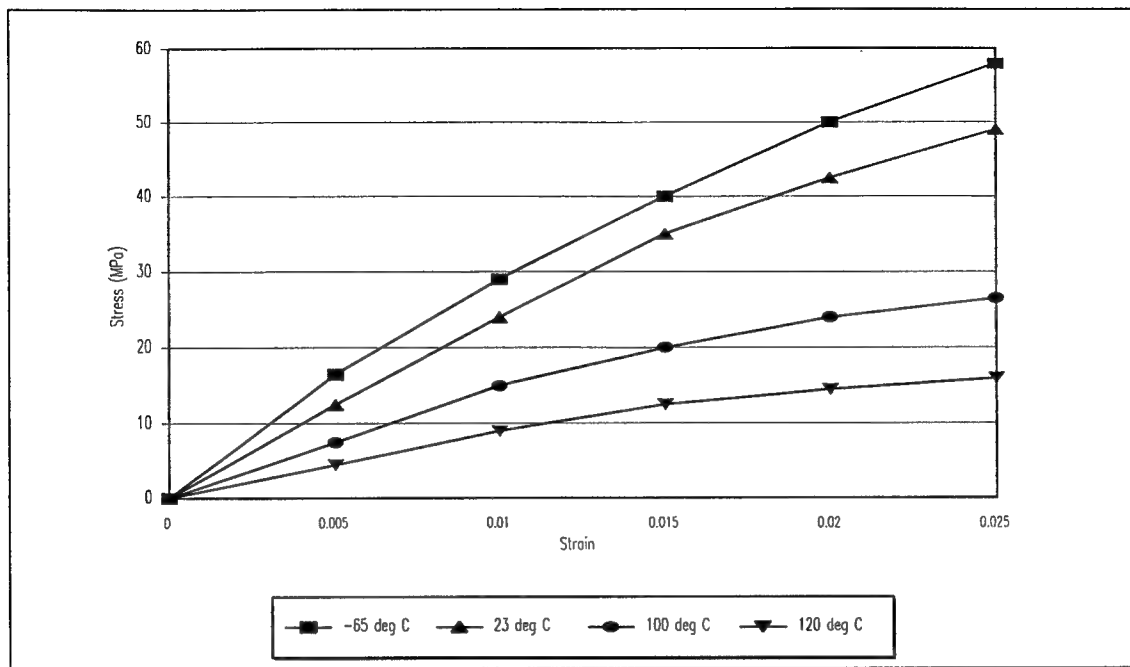


Figure 38. True Stress vs. True Strain curves for SPI EPOXY. [4]

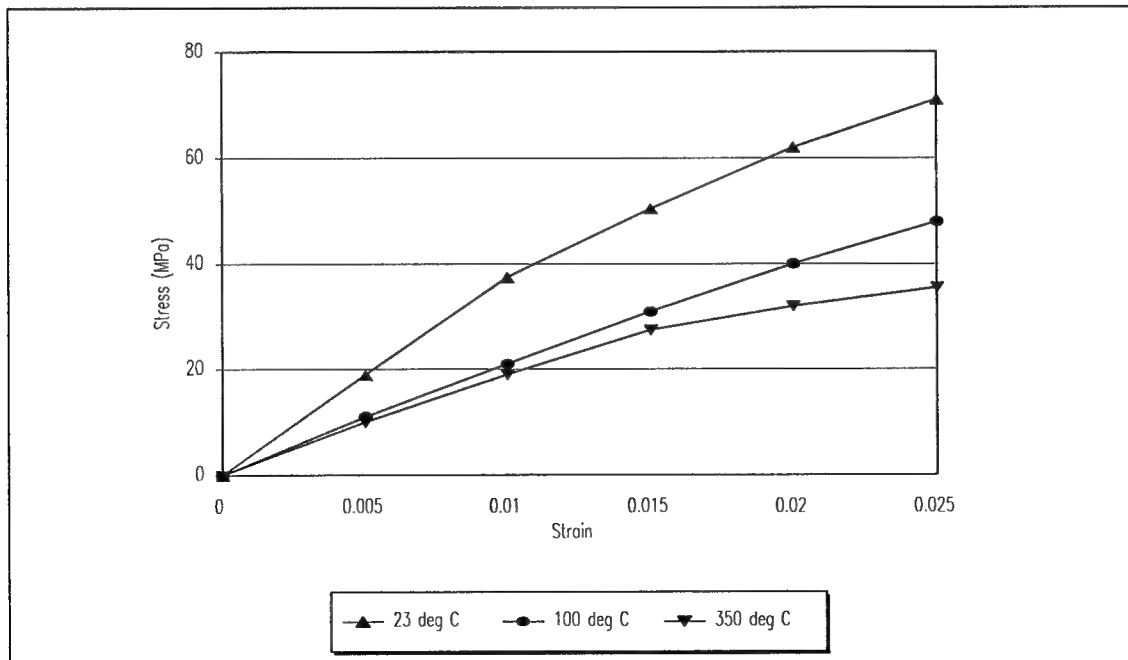


Figure 39. True Stress vs. True Strain curves for SDAN. [5]

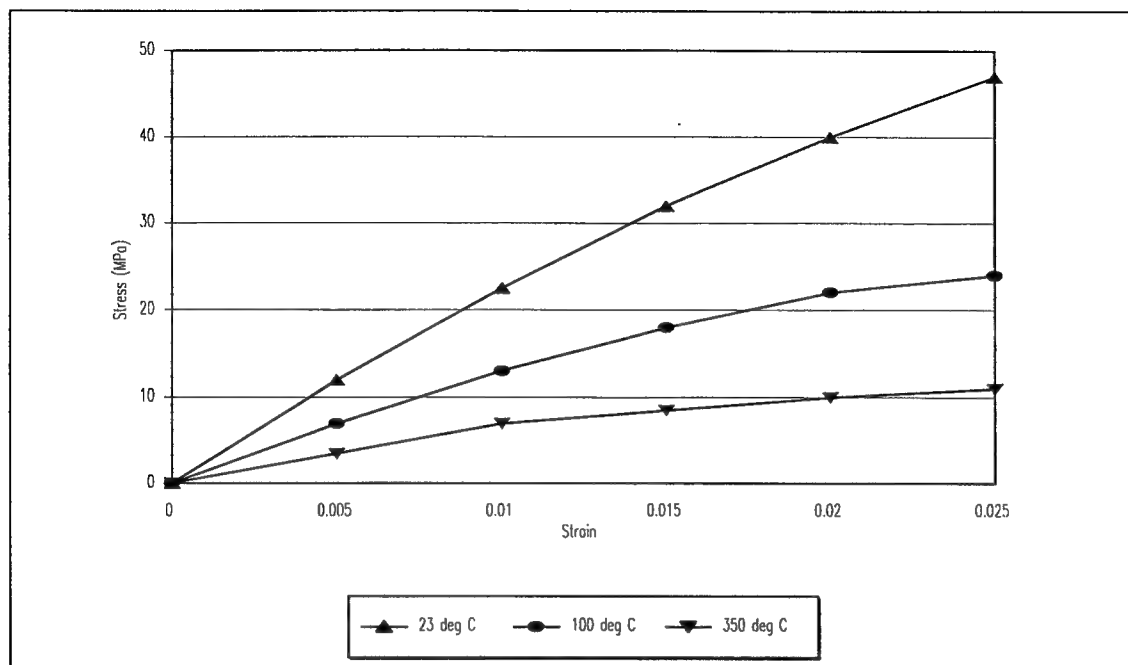


Figure 40. True Stress vs. True Strain curves for SE45. [5]

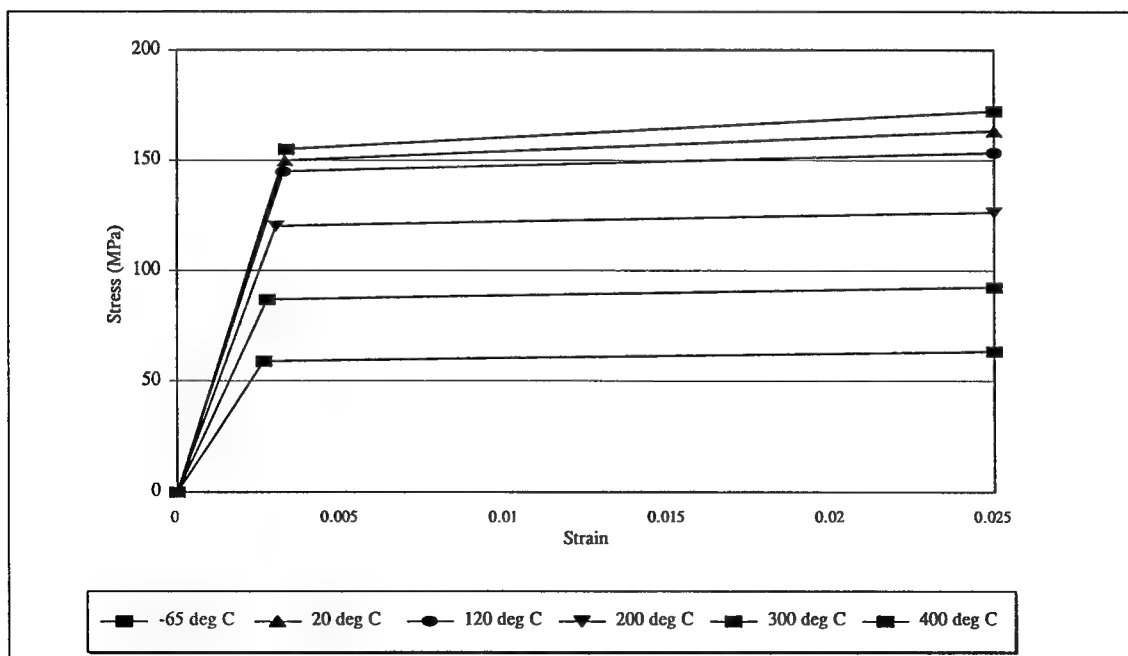


Figure 41. True Stress vs. True Strain curves for copper. Data provided by IBM electronics division at Endicott, NY, based upon in-house testing.

## APPENDIX C

### DERIVATION OF THE ANALYTICAL MODEL

The analytical model of the strain is created by solving the equations for sum of forces ( $\Sigma F$ ), and sum of moments ( $\Sigma M$ ). Below are the assumptions, and the derivation of the model:

Assumptions: -Planes remain planes

-Plane stress

-Linear material properties

-No external forces, so that  $\Sigma F = \Sigma M = 0$

-Uniform temperature

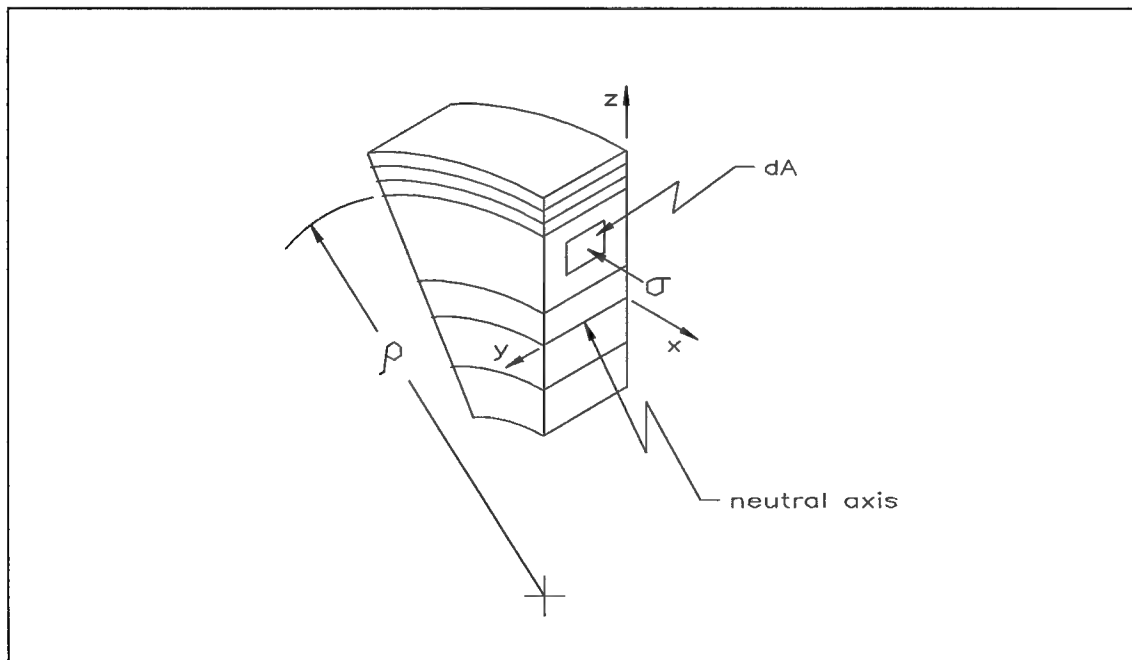


Figure 42. Schematic showing a portion of a generic layered solid in bending.

Using  $\Sigma F = 0$  and assuming small strains and displacements, we have:

$$\Sigma F_x = 0 = \int_A \sigma_x dA \quad (7)$$

where  $\sigma_x$  is stress in the x direction, and  $dA$  is an infinitesimally small area. Assuming plane stress, and linear materials:

$$\sigma_x = E \epsilon_{el} \quad (8)$$

where  $E$  is Young's Modulus, and  $\epsilon_{el}$  is the elastic strain. Note that the elastic strain is only one component of the total strain. The total strain is given by:

$$\epsilon_{tot} = \epsilon_{el} + \epsilon_{therm} \quad (9)$$

where  $\epsilon_{tot}$  is the total strain, and  $\epsilon_{therm}$  is the thermal strain. Solving Eq. 9 for  $\epsilon_{el}$ , and substituting into Eq. 3, we get

$$\Sigma F_x = 0 = \int_A E(\epsilon_{tot} - \epsilon_{therm}) dA \quad (10)$$

From the assumption that planes remain plane, we find that the total strain [11] is:

$$\epsilon_{tot} = \frac{z}{\rho} + \epsilon_n \quad (11)$$

where  $z$  is the distance from the neutral axis,  $\rho$  is the radius of curvature of the neutral axis, and  $\epsilon_n$  is the strain of neutral axis due to internal forces. Also note that the thermal strain is given by:

$$\epsilon_{therm} = \alpha \Delta T \quad (12)$$

where  $\alpha$  is the coefficient of thermal expansion, and  $\Delta T$  is the change in temperature from the stress free reference temperature. Substituting Eqs. 11 and 12 into Eq. 10 and recognizing that different layers have different material properties, one has:

$$\Sigma F_x = 0 = \sum_{i=1}^m \left( \int E_i \epsilon_n dA_i + \int \frac{E_i}{\rho} z dA_i - \int E_i \alpha_i \Delta T dA_i \right) \quad (13)$$

where subscript  $i$  is an individual layer,  $m$  is the total number of layers. We recognize that  $E_i$ ,  $\epsilon_n$ ,

$\rho$ ,  $\alpha_i$ , and  $\Delta T$  are not a functions of  $A_i$ , and that  $\int z dA_i = \bar{z} A_i$ . Therefore Eq. 13 becomes:

$$\Sigma F_x = 0 = \epsilon_n \sum_{i=1}^m E_i A_i + \frac{1}{\rho} \sum_{i=1}^m E_i \bar{z}_i A_i - \Delta T \sum_{i=1}^m E_i \alpha_i A_i \quad (14)$$

where  $\bar{z}_i$  is the distance of centroid of layer  $i$  from neutral axis. Note that  $\Sigma E_i \bar{z}_i A_i = 0$  from the derivation of the location of the neutral axis, (to be shown later). Also we note that the width of the MCM is constant so that  $A_i$  can be replaced by  $h_i$ , the height of a layer. Using this and solving Eq. 14 for  $\epsilon_n$ , we get:

$$\epsilon_n = \frac{\sum_{i=1}^m \alpha_i E_i h_i}{\sum_{i=1}^m E_i h_i} \Delta T \quad (15)$$

From here we move on to the  $\Sigma M$  equations.

$$\Sigma M_y = 0 = \int_A \sigma_x z dA \quad (16)$$

Again, assuming plane stress, linear materials, and using Eq.9 we get:

$$\Sigma M_y = 0 = \int_A E(\epsilon_{tot} - \epsilon_{therm}) z dA \quad (17)$$

Again we use Eq. 11 and 12, and substitute into 27 to get:

$$\Sigma M_y = 0 = \epsilon_n \sum_{i=1}^m E_i \int_A z dA_i + \frac{1}{\rho} \sum_{i=1}^m E_i \int_A z^2 dA_i - \Delta T \sum_{i=1}^m E_i \alpha_i \int_A z dA_i \quad (18)$$

Recall that  $\int z dA_i = \bar{z}_i A_i$ , and that  $\int z^2 dA_i = \bar{I}_i A_i$  so that we get:

$$\Sigma M_y = 0 = \epsilon_n \sum_{i=1}^m E_i \bar{z}_i A_i + \frac{1}{\rho} \sum_{i=1}^m E_i \bar{I}_i - \Delta T \sum_{i=1}^m E_i \alpha_i \bar{z}_i A_i \quad (19)$$

where,  $\bar{I}_i$  is the area moment of inertia of a layer about the neutral axis. Now using the parallel axis theorem, we get:

$$\bar{I}_i = I_i + \bar{z}_i^2 A_i \quad (20)$$

where,  $I_i$  is the area moment of inertia of a layer about it's own neutral axis. We use the fact the

$I_i = bh_i^3/12$ ,  $A_i = bh_i$ , and we again recognize that  $\Sigma E_i \bar{z}_i A_i = 0$ , to get:

$$\Sigma M = 0 = \frac{1}{\rho} \sum_{i=1}^m E_i h_i \left( \frac{h_i^2}{12} + \bar{z}_i^2 \right) b - \Delta T \sum_{i=1}^m E_i h_i \alpha_i \bar{z}_i b \quad (21)$$

where  $b$  is the width of MCM

We solve Eq. 21 for  $1/\rho$ :

$$\frac{1}{\rho} = \frac{\sum_{i=1}^m E_i h_i \alpha_i \bar{z}_i}{\sum_{i=1}^m E_i h_i \left( \frac{h_i^2}{12} + \bar{z}_i^2 \right)} \Delta T \quad (22)$$

Recall that the total strain is given by:

$$\epsilon_{tot} = \frac{z}{\rho} + \epsilon_n \quad (11)$$

Therefore:

$$\epsilon_{tot} = \alpha_{tot} \Delta T \quad (23)$$

where,

$$\alpha_{tot} = \frac{\sum_{i=1}^m E_i h_i \alpha_i \bar{z}_i}{\sum_{i=1}^m E_i h_i \left( \frac{h_i^2}{12} + \bar{z}_i^2 \right)} \bar{z} + \frac{\sum_{i=1}^m E_i h_i \alpha_i}{\sum_{i=1}^m E_i h_i} \quad (5)$$

Hence, the equation for the elastic strain is given by:

$$\epsilon_{el} = (\alpha_{tot} - \alpha_i) \Delta T \quad (4)$$

The only part of the analytical model still remaining is the derivation of the location of the neutral axis, and the reason why  $\sum E_i h_i \bar{z}_i = 0$ .

The location of the neutral axis with respect to arbitrary point P is given as follows

$$\bar{Z}^P = \frac{\sum_{i=1}^m E_i h \bar{z}_i^P}{\sum_{i=1}^m E_i h_i} \quad (24)$$

where  $\bar{Z}^P$  is the location of centroid of MCM with respect to P,  $\bar{z}_i^P$  is the distance of centroid of layer  $i$  with respect to P. As can be seen, if point P is on the neutral axis then  $\bar{Z}^P = 0 = \sum E_i h_i \bar{z}_i^P$ , and that  $\bar{z}_i^P = \bar{z}_i$ .



## APPENDIX D

### DERIVATION OF VARIOUS FORMULAE

#### 1. Relationship of Out-of-plane Strain to Average In-Plane Strain

- Assumptions:
- 1)  $\sigma_z = 0$
  - 2) linear properties
  - 3) All material properties are isotropic, except the CTE.

Assumption (1) is justified because there is nothing to provide constraint in the z direction (ignoring the vias), so that the z stress must be zero. Assumptions (2-3) are consistent with the assumptions used in the shell model.

Using Generalized Hooke's Law with  $\sigma_z = 0$  we have:

$$\epsilon_{x\_tot} = \frac{1}{E}(\sigma_x - \nu\sigma_y) + \alpha\Delta T \quad (25)$$

$$\epsilon_{y\_tot} = \frac{1}{E}(\sigma_y - \nu\sigma_x) + \alpha\Delta T \quad (26)$$

$$\epsilon_{z\_tot} = \frac{-\nu}{E}(\sigma_x + \sigma_y) + \alpha_z\Delta T \quad (27)$$

where  $\epsilon_{i\_tot}$  = total strain in the i direction,  $\alpha$  = CTE in the x and y direction, and  $\alpha_z$  = CTE in the z direction. Adding 25 and 26) we get:

$$\epsilon_{x\_tot} + \epsilon_{y\_tot} = 2\alpha\Delta T + \frac{1}{E}((\sigma_x + \sigma_y)(1 - \nu)) \quad (28)$$

Solve for  $(\sigma_x + \sigma_y)$ :

$$\sigma_x + \sigma_y = \frac{E}{1-\nu}((\epsilon_{x\_tot} + \epsilon_{y\_tot}) - 2\alpha\Delta T) \quad (29)$$

Substitute 29) into (27) we get:

$$\epsilon_{z\_tot} = \frac{\nu}{1-\nu}(2\alpha\Delta T - (\epsilon_{x\_tot} + \epsilon_{y\_tot})) + \alpha_z\Delta T \quad (30)$$

Since  $\epsilon_{In\_Plane\_Avg.} = \frac{1}{2}(\epsilon_{x\_tot} + \epsilon_{y\_tot})$ , we have defined the out-of-plane strain as a function of the average in-plane strain. Note that the first term in Eq. (30) represents the elastic strain, while the second term represents the thermal strain.

## BIBLIOGRAPHY

- [1] G. L. Ginsberg and D. P. Schnorr, "Multichip Modules and Related Technologies", McGraw Hill, New York, (1994)
- [2] S. Rupley and J. Clyman, "P6: The Next Step", PC Magazine, pp. 104-118 (Sept. 1995)
- [3] A. Isobe, M. Shinohara, M. Hiraki and A. Hoshino, " Via Hole Failure Study", NEC Research and Development, Vol. 34, No. 1, (1993)
- [4] A. S. Prabhu, D. B. Barker and M.G. Pecht, "A Thermo-Mechanical Fatigue Analysis of High Density Interconnect Vias", Advances in Electronic Packaging, ASTM EEP 10-1, Vol 10, pp. 187-216, (1995).
- [5] X. Wu, M. Li, M. Pecht, "An Experimental Study of Polyimide Films Used in HDI Interconnects," CALCE Electronic Packaging Research Center, University of Maryland, College Park, MD 20742
- [6] R. E. Peterson, "Stress Concentration Design Factors", John Wiley and Sons, Inc., New York, (1953).
- [7] W. Engelmaier, "A Method for the Determination of Ductility for Thin Metallic Materials," Formability of Metallic Materials - 2000 A. D. , ASTM STP 753, J. R. Newby and B. A. Niemeier, Eds., American Society for Testing and Materials, pp. 279-295, (1982).
- [8] I. Grosse, P. Katragadda and A. Jog, "Knowledge Sources for an Intelligent MCM Analyzer," University of Massachusetts, Final Technical Report for Rome Laboratory, RL-TR-93-123, (June 1993).
- [9] U. S. Military Specification MIL-STD-883
- [10] D. Read and E. Drexler et al, "Thermomechanical Behavior of a High Density Polymer Overlay MCM Interconnect Structure: Experiments and Analysis", 1995 International Mechanical Engineering Congress and Exposition, San Francisco, (Nov.1995)
- [11] Beer and Johnson, "Mechanics of Materials," McGraw-Hill Co., New York, (1981)

***MISSION  
OF  
ROME LABORATORY***

**Mission.** The mission of Rome Laboratory is to advance the science and technologies of command, control, communications and intelligence and to transition them into systems to meet customer needs. To achieve this, Rome Lab:

- a. Conducts vigorous research, development and test programs in all applicable technologies;
- b. Transitions technology to current and future systems to improve operational capability, readiness, and supportability;
- c. Provides a full range of technical support to Air Force Materiel Command product centers and other Air Force organizations;
- d. Promotes transfer of technology to the private sector;
- e. Maintains leading edge technological expertise in the areas of surveillance, communications, command and control, intelligence, reliability science, electro-magnetic technology, photonics, signal processing, and computational science.

The thrust areas of technical competence include: Surveillance, Communications, Command and Control, Intelligence, Signal Processing, Computer Science and Technology, Electromagnetic Technology, Photonics and Reliability Sciences.